Astron. Astrophys. 321, 268–287 (1997)

ASTRONOMY
AND
ASTROPHYSICS

Photon loss from the helium Lyα line – the key to the acceleration of Wolf-Rayet winds

W. Schmutz

Institut für Astronomie, ETH-Zentrum, CH-8092 Zürich, Switzerland

Received 15 February 1995 / Accepted 1 October 1996

Abstract. It is demonstrated that the ionization equilibrium of helium in non-LTE atmospheres for Wolf-Rayet stars is very sensitive to photon loss from the He II Lyα line. A removal of 0.001% of the photons is sufficient to initiate an abruptly recombining ionization equilibrium. The assumption of photon loss allows to address the wind momentum problem of Wolf-Rayet stars. It is possible for the first time to construct a line blanketed non-LTE model of a Wolf-Rayet star that reproduces the observed spectrum and simultaneously, provides the radiation force to drive its outer velocity structure.

A method is developed to determine the free model parameters L, $R_{\rm phot}$, $\dot{M}$, v_∞, $v_{\rm phot}$, C (clumping factor), and f (photon loss factor), by an analysis of an observed Wolf-Rayet spectrum. The method is applied to the spectrum of the WN5 star HD 50896 resulting in good fits in shape and strength to the observed helium emission lines. In particular the profile of the He I λ10830 line, which is a tracer of the outer velocity structure, is reproduced remarkably well. The hydrodynamically calculated velocity law differs significantly from the commonly adopted β-law with $\beta = 1$. The outer part can be approximated by a β-law with $\beta = 3$ if the core radius of the atmosphere model is used, or by $\beta = 8$, if the velocity law is calculated referring to the hydrostatic radius of a stellar evolution model in the Wolf-Rayet phase. Close to the photosphere the velocity structure is flat with an expansion velocity of $v_{\rm phot} \approx 1100$ km s^{-1}. The resulting luminosity $L = 5.5 \cdot 10^5$ L$_\odot$ and terminal wind velocity $v_\infty = 2060$ km s^{-1} are found to be considerably larger than the values from previous determinations. On the other hand, the mass loss rate is lower $\dot{M} = 3.2 \cdot 10^{-5}$ M$_\odot$yr^{-1} due to an inhomogeneous wind with a clumping factor $C \approx 4$. There is evidence for a decrease of the clumping factor with distance from the star.

The photon loss factor is determined empirically to have a value of $f \approx 10^{-4}$. It is proposed that a Bowen resonance-fluorescence mechanism removes a small fraction of photons from the radiation field of the helium Lyα resonance line. Photon loss calculated theoretically from the interaction of metal lines close in wavelength to the He II Lyα line yields a depth dependent factor in the range $10^{-4} \ldots 10^{-3}$. In the recombination zone, where the photon loss influences the ionization structure, its value is $f^* \approx 10^{-4}$ in excellent agreement with the empirically determined value. The lines Ca V λ303.74, Fe VI $\lambda\lambda$303.70, 303.80, 303.83, and O III λ303.80 are roughly of equal importance.

The wind momentum calculated by the present model exceeds the single scattering limit by a factor of 6 in contrast to previous estimates that yielded factors 50 – 100. With a momentum ratio of 6 the Wolf-Rayet winds are no longer distinct from other radiation driven winds but they fit as more extreme versions to the winds of O stars.

Key words: hydrodynamics – radiative transfer – methods: numerical – stars: HD 50896 – stars: mass-loss – stars: Wolf-Rayet

1. Introduction

In a recent paper Lucy & Abbott (1993; hereafter LA) presented calculations that explained the driving of a Wolf-Rayet wind by radiation pressure. Their result is in striking contrast to the conclusions of Puls & Pauldrach (1991) and Schmutz (1994) who found that the radiation force is insufficient to drive the mass loss. This contradiction is, in fact, surprising if one realizes that both LA and Schmutz (1994), calculate the radiation force with the same Monte Carlo technique, based on the work by Abbott & Lucy (1985). LA argue that the change of ionization in the wind is the reason for a large efficiency of momentum transfer. However, it can be shown (Schmutz 1995) that LA have not identified the correct reason for their success. Schmutz & Hamann (1986) have realized that helium recombines in the wind when the first non-LTE atmospheres for Wolf-Rayet stars have been calculated. Since then, the ionization stratification of helium is the standard diagnostic tool to analyze Wolf-Rayet spectra. Thus, an ionization change is present in almost all non-LTE models. Nevertheless, they do not provide enough force to drive their winds (Schmutz 1994). It is certainly true that an ionization stratification is a necessary condition but, as the investigations of Puls & Pauldrach (1991) and Schmutz (1994) reveal, it is not a sufficient condition for efficient driving. A detailed comparison

of the LA model with non-LTE calculations reveals the reason for the success of LA's calculation: LA adopted an ionization structure which drastically differs from that obtained by solving the rate equations in a model atmosphere. In the LA model the recombination of helium (and correspondingly of metals) is almost immediate whereas in the non-LTE models recombination occurs very gradually (Schmutz & Hamann 1986; Hillier 1988). At this point, it is important to stress that Puls & Pauldrach (1991) and Schmutz (1994), who found insufficient force to drive the Wolf-Rayet winds, used models that reproduce the observed Wolf-Rayet spectra, whereas LA do not predict any spectra. Based on this difference one is tempted to declare the LA model as less reliable because they do not test their calculations against observations. However, such a judgment would not do justice to their calculation. It was extremely important that LA found a way to get radiation pressure to drive a WR wind. Since the crucial difference is that LA treated recombination as an independent variable, whereas earlier work obtained recombination from model calculations, this immediately suggested that the basic assumptions for the calculation of recombination needed re-evaluation. As shown by Schmutz (1995), a small loss of photons from the He II Lyα line is sufficient to drastically alter the ionization structure. Resonance absorption by another species is a viable candidate for producing such a loss. Thus, it appears that photon loss from the helium Lyα line is the key process to understand the Wolf-Rayet winds.

In this work I report on a new aspect of this hypothesis. I still propose that photon loss from the He II λ303 to be the crucial process to understand the acceleration of Wolf-Rayet winds. However, the new calculations reported below indicate a different type of solution than aimed at in Schmutz (1995). There, the idea was that it is possible to obtain large momentum transfer efficiencies from a fast recombining ionization structure. Now, I advocate solutions with almost "normal" momentum transfer efficiencies. It is possible to construct a model that reproduces the spectrum of a Wolf-Rayet star with strong lines with $\dot{M}v_\infty/(L/c)$ ratios of only a few times unity instead of factors like 30 up to 100 as thought to be necessary for Wolf-Rayet stars (Hamann et al. 1993). With this type of solution, the Wolf-Rayet winds are just a more extreme extension of strong O star winds and no longer a class on their own. An important new aspect of the solution reported here is that due to the photon loss, spectroscopic analyses of the spectra yield higher luminosities for Wolf-Rayet stars. Thus, part of the wind momentum problem of Wolf-Rayet stars is solved by increasing their luminosities. Another contribution comes from the assumption of clumping, and a third contribution is obtained by splitting the problem into two parts of about equal magnitude: the acceleration within the optically thick atmosphere and the acceleration in the optically thin part. Here, I only investigate the acceleration of the wind in the optically thin atmosphere, and I leave the question open what mechanism creates and accelerates the wind in the optically thick layers. Observations show that the winds of Wolf-Rayet stars with strong lines already expand with about half the terminal velocity at the photosphere (Willis 1982). Although with the present work the Wolf-Rayet momentum problem is only partly solved, it is nevertheless for the first time that a model for a Wolf-Rayet atmosphere is presented with the outer velocity structure calculated hydrodynamically.

In the next Section I describe how the models are calculated and the general fitting procedure is outlined. In Sect. 3, I present a model that reproduces the spectrum of the Wolf-Rayet star HD 50897 (EZ CMa) and simultaneously provides the radiation force to accelerate its wind in the optically thin region. In Sect. 4 the photon loss factor is evaluated theoretically and compared with the value determined empirically in Sect. 3. The results of the present work are discussed in Sect. 5 and the conclusions are presented in Sect. 6.

2. Method

2.1. Numerical calculations

A hydrodynamic Wolf-Rayet atmosphere is obtained in three steps that are repeated and iterated to consistency. The first step is the calculation of a H/He non-LTE atmosphere. This computation is performed with the comoving frame code developed in Kiel (Hamann & Schmutz 1987; Wessolowski et al. 1988) using the Λ-iteration technique of Hamann (1987). The next step is a formal solution of the radiation transfer with Monte Carlo simulation including tens of thousands of spectral lines. This code is a version of that of Abbott and Lucy (1985), modified to include the non-LTE ionization structure and opacities from the non-LTE atmosphere (Schmutz 1991). The third step is the solution of the equation of motion (Castor et al. 1975) given the CAK parameters α and k that are obtained from the Monte Carlo radiation transfer. The full procedure is described in more detail in Schaerer & Schmutz (1994).

An important aspect of the above procedure is that in contrast to all other hydrodynamical calculations of stellar winds from hot stars, the evaluation of the radiation force and the transfer problem are treated consistently. The radiation field determined by the non-LTE solution of the transfer problem is used for the calculation of the radiation force and vice versa, the line blanketing found in the Monte Carlo solution is taken into account in the non-LTE atmosphere. For O stars, this consistent evaluation of the force has been presented by Schaerer & Schmutz (1994). There, the new approach yielded solutions that are not dramatically different from less sophisticated calculations. However, because of the large optical depths in a Wolf-Rayet wind a consistent treatment is essential.

Here, in contrast to the full hydrodynamic solutions in the paper by Schaerer & Schmutz (1994), which includes the solution of the critical point equations, it is only attempted to solve for the acceleration of the Wolf-Rayet wind. It is assumed that the mass loss is created and accelerated to something like half the terminal velocity by an unknown mechanism. The velocity law in the optically thick part of the atmosphere is specified by a β-law and only the outer part of the velocity law is calculated.

The atmosphere models presented here include two new features: 1) the models account for clumping, although only a

crude approximation is used and 2) photon loss from the He II Lyα line is assumed.

2.1.1. Clumping

Time dependent solutions of radiation driven stellar winds predict density inhomogeneities (Owocki et al. 1988; Rybicki et al. 1990; Feldmeier 1995). Theory predicts that the clumping factor is of the order of three. There is also some observational evidence that Wolf-Rayet winds are clumped (e.g. Moffat & Robert 1994; Cherepashchuk et al. 1995). A clumping factor of 3 has been derived by Moffat & Robert (1994), but because the observations are very difficult to interpret, it is not evident whether the observational data are really in contradiction with homogeneous mass loss. In the present models the clumping factor is treated as a free parameter. Only the high density part is taken into account. The density within a clump is obtained from the mean density by a multiplication with a clumping factor C. The mean density is derived from the mass loss rate and the expansion velocity at a given location requiring mass conservation. The low density regions are assumed to be completely transparent and they are neglected. This simple assumption is justified to first order by the results of Owocki et al. (1988) (see also Owocki 1991) who found a steep transition between low and high density regions and that the average density is dominated by the high density regions. In practice, this approximate treating of clumping is realized by specifying a continuous density distribution that is enhanced from the mean density by the given factor and by reducing by the same factor all dimensions when used for radiation transfer calculations.

For the Monte Carlo radiation transfer, where the lines are treated with the Sobolev approximation, it is assumed that the clumping scale is small compared with the Sobolev length. This statement is sufficient to specify the modification to the code. It implies that the mean density is used for the evaluation of the Sobolev optical depth. This treatment represents a limiting case where the physical size of the clumps does not play a role. The other limiting case would be to assume that the Sobolev length is small compared to the clump size. In this case, it would be necessary to evaluate whether a line scattering occurs within a clump. The choice between this two cases was based on the result that the chosen method yields the larger radiative force. So far, there is no observational indication that would favor one case above the other.

2.1.2. Photon loss

Photon loss from the He II λ303 line has been proposed by Schmutz (1995) to be the key process to understand the Wolf-Rayet winds. This hypothesis is based on the empirical result that in non-LTE calculations, the helium ionization structure is extremely sensitive to a small modification of the mean intensity averaged over the line profile of this line. Fig. 1 illustrates the dependence of the helium ionization structure on photon loss. In the rate equation the line radiation field is modified by a factor $(1-f)$: $\bar{J}^{\rm rate} = (1-f)\,\bar{J}^{\rm line}$, where f is the fraction of photons

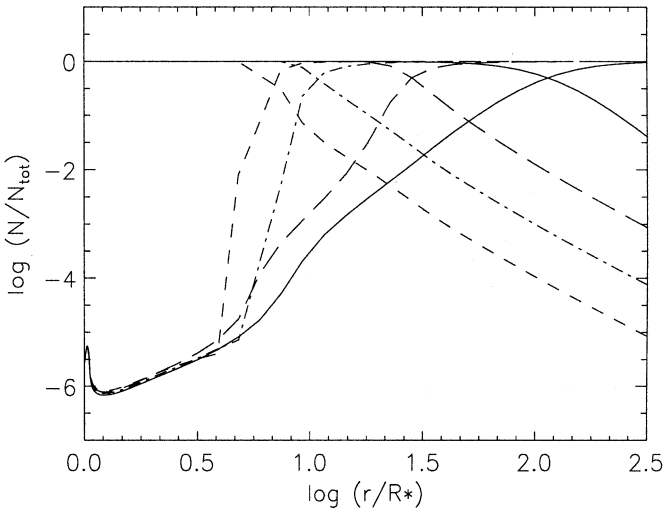

Fig. 1. Effect of photon loss from the He II λ303 resonance line on the ionization structure of helium. The line styles denote different photon loss factors: full drawn lines – no photon loss; long dashed lines – $f = 10^{-5}$; dashed-dotted lines – $f = 10^{-4}$; dashed lines – $f = 10^{-3}$. Plotted are the relative populations of levels, N(He^{++})/N$_{\rm He}$ (the lines with value 1 at small radii) and N(He^{+} n=1)/N$_{\rm He}$. The two populations from the same model are drawn with the same line style.

that are lost from the He II transition. More exactly, I use the formulation $\bar{J}^{\rm rate} = (1-f)\,(\bar{J}^{\rm line} - B(T_e)) + B(T_e)$, where $B(T_e)$ is the Planck function of the local electron temperature. This formulation ensures that at large optical depth the LTE case with no photon loss is recovered (cf. Eq. A13). In this form the factor f corresponds to the capture factor $f^{\rm cap}$ of Eq. A7. However, in practice, it is found that $\bar{J}^{\rm line} > S^{\rm m_i} >> B(T_e)$ in the regions where photon loss is important. Therefore, the factor f that is determined empirically corresponds to the the photon loss factor f^* of Eq. A4 that accounts for both the capture of helium line photons and contribution of photons from metal line transitions. Thus, the more simple formulation $\bar{J}^{\rm rate} = (1-f)\,\bar{J}^{\rm line}$, reflects the actual modification to the rate equation in the region where the modification plays a role.

Even very small loss factors such as $f = 10^{-5}$ considerably change the ionization structure of helium. In Fig. 1 it can be seen that the inner part of the atmosphere is not affected. There is a certain point from which a more rapid recombination of helium sets in due to the photon loss factor. This is the location in the atmosphere where the He^{+} ground level is basically isolated in the rate equation system except for large rates to and from He^{+} n=2. The populations of He^{+} n=2 and the higher levels of He^{+} are well determined by bound-bound processes among these levels and ionization to and recombination from He^{++}. Therefore, these levels are not affected by photon loss from the He II λ303 resonance line. However, the He^{+} ground state changes its population until the next larger rate is able to compensate the fraction lost from the radiative excitation to $n = 2$.

I propose that the physical process responsible for the photon loss is the interaction of the radiation field of the helium line with metal line transitions. A fraction of the line photons

get lost by exciting an iron level and escape via a branch of the numerous (optically thin) transitions to other iron levels. In Sect. 4 the value of the photon loss factor is calculated theoretically. However, the identification of the agent responsible for the process is not central to this paper. In the model atmosphere calculations of Sect. 3, the photon loss factor is treated as a free parameter. Thus, the results of Sect. 3 do not depend whether or not the correct reason for photon loss is identified. For the model atmosphere calculations, the only important fact is *the numerical result that the ionization equilibrium in the wind is very sensitive to small perturbations of the line radiation field.* If such a sensitivity exists then it is very unlikely that in reality the undisturbed result is realized.

2.2. Fitting procedure

It is not at all straightforward to find a model that reproduces the observed line profiles of a Wolf-Rayet star and simultaneously provides the force for the acceleration of its wind. There are, in total, nine free parameters that have to be determined. A "standard" spectroscopic analysis, i.e. an analysis using model atmospheres without hydrodynamically calculated density structures, has four free parameters, T_*, R_*, dM/dt, and v_∞ (Schmutz et al. 1989). These parameters are the effective temperature, T_*, referred to the radius of the inner model boundary, R_*, the mass loss rate, dM/dt, and the terminal velocity of the wind, v_∞. It should be noted however, that in a standard analysis it has never been attempted to determine the velocity law. The velocity law is always specified – usually with a β-law – and this assumption is equivalent to as many free parameters as there are depth points in the model atmosphere. Thus, strictly speaking, the nine free parameters used here are much less than implicitly needed for a standard analysis.

The solution of the hydrodynamic equation has as free parameter the stellar mass M. The solution presented here does not include the part of the velocity structure where the critical point is located. Therefore, two boundary values have to be specified: the terminal velocity v_∞, and a value at the inner boundary of the hydrodynamic solution, $v_{\rm phot}$. For deeper layers than this boundary the velocity law is specified by the parameter β.

The only parameters that are in addition to those usually used for a spectroscopic analysis are the parameters to account for clumping, the clumping factor C, and for photon loss, the factor f.

In the following subsections, I describe the procedure to determine these parameters.

2.2.1. Photospheric and terminal expansion velocity

The seemingly easiest parameter to determine from the spectrum is the terminal velocity of the wind, v_∞. Indeed, a good starting value can be measured directly from the spectrum. However, if line fits are attempted, then better values are required. One difficulty is that the radial velocity of a Wolf-Rayet star cannot be obtained directly from the spectrum because the line profiles are not symmetric. Thus, the reference wavelength λ_0 to which the width of the line has to be measured is not known. In addition, even the almost box-shaped He I lines have inclined line wings that depend on the velocity law. Thus, for values more precise than a few 100 km s^{-1} the terminal velocity has to be determined by comparing observed lines with synthetic profiles. This implies that the terminal velocity is revised with each iteration of the velocity law.

Similarly, as for the terminal velocity, a first guess for the photospheric expansion velocity, $v_{\rm phot}$, can be obtained to an accuracy of a few 100 km s^{-1} by measuring the widths of the narrowest lines. The best lines to use are the weakest He II lines (see Willis 1982). But again, only line fits yield more exact values, i.e. also $v_{\rm phot}$ has to be updated each iteration.

2.2.2. Mass loss rate and clumping

The line strengths depend on the density in the line formation regions and, indirectly, on the mass loss rate. Hillier (1991b) has pointed out that the line strength is a quadratic function of the density in the wind but that the electron scattering wings are a linear measure of the mass loss rate. Thus, fits to the electron scattering wings yield the mass loss rate and the line strength can be reproduced by adjusting the clumping factor, C.

2.2.3. Photon loss factor

In contrast to a "standard" analysis of the Wolf-Rayet spectrum, where the stellar temperature results from the line ratio of a He I and a He II line, the stellar temperature in this analysis cannot be determined from the spectrum. The difficulty lies within the effect of the photon loss parameter. As can be seen in Fig. 1 the relative size of the regions, where He^{++} and He^{+} are the dominant ionization stages, changes drastically when the photon loss parameter is varied. Since the strengths of He I and He II lines basically result from the amount of mass that is in the He^{++} and He^{+} zones, different values of f yield different strengths of the He I and He II lines and, in particular, the ratio of the line strengths of He I to He II changes. Exactly the same influence is found when the stellar temperature is varied. Thus, from the spectrum, only the *combination* of the two parameters, T_* and f, can be determined but not the individual ones. As will be discussed below, the stellar temperature is determined in a different way. The observed He I to He II line ratio is used to estimate the photon loss factor f.

2.2.4. Luminosity and stellar radius

The hydrodynamic equation provides the velocity structure but in addition, and equally important, the hydrodynamic equation yields a relation between luminosity and mass loss rate. In the usual applications of hydrodynamic calculations to stellar winds, the stellar parameters are known and a mass loss rate is obtained. Here, however, the mass loss rate is determined by fitting the electron scattering line wings. Therefore, the hydrodynamic solution can be used to determine the luminosity for given mass loss rate and given boundary values for the velocity.

The stellar radius, R_*, results from the requirement that the model has to fit the observed flux at given wavelength. A model can be scaled simply to the desired magnitude using the relations given by Howarth & Schmutz (1992). However, it should be noted that the stellar radius is only an inner boundary of the atmosphere model. Since the location of the inner radius depends on the velocity law at large optical depths, and because this law is not obtained from a hydrodynamical solution, this radius is rather arbitrary. Correspondingly, the effective temperature that is derived from the luminosity and radius via the relation $\sigma T_*^4 = L/4\pi R_*^2$ is also not well defined. This topic has been discussed in more detail by Schmutz et al. (1992).

2.2.5. Inner velocity law and stellar mass

Guided by the results for optically thick winds in nova outbursts (e.g. Kato & Hachisu 1994), I assumed that the creation of the Wolf-Rayet wind takes place deep in the atmosphere and that there, at the base of the wind, it is accelerated quickly. Therefore, I have adopted for the velocity law in the inner part a steep law using $\beta = 0.5$. So far, I have not found an observational constraint to estimate the value of this parameter and I have kept it fixed throughout this paper. The last of the nine parameters, the stellar mass M, is also not treated as a free parameter. It is obtained from the luminosity using the theoretical mass-luminosity relation for Wolf-Rayet stars (Schaerer & Maeder 1992).

3. Results

The aim of the calculations presented in this section is to construct a model atmosphere that reproduces the observed line profiles of the Wolf-Rayet star HD 50896 (WR6) and simultaneously, provides the force to accelerate the wind in the optically thin part.

Five parameters result from fits to the observed line profiles: the terminal wind velocity v_∞, the wind velocity at the photosphere $v_{\rm phot}$, the mass loss rate $\dot{M}$, the clumping factor C, and the photon loss factor f. These parameters are determined for given luminosity and stellar radius. The later two parameters are found from the hydrodynamic solution.

3.1. The terminal velocity

In Fig. 2 the profiles predicted by models with two different terminal velocities are compared with the observed He I λ10830 line. Given the very good agreement of the observed profile with the synthetic profile, it can be concluded that for most of the material the terminal velocity is 2060 km s^{-1}±50 km s^{-1}. There is some excess emission on the red wing of the He I line that extends to 2400 km s^{-1}. The interpretation of this feature is not straightforward. A plausible explanation is that we see the signature of low density material that is not included in the present model. The fact that it reaches a higher terminal velocity than the high density material would indicate that there are radial directions containing only low density gas. Alternatively, the excess emission in the red wing could also be due to an imperfect reproduction of the He II line λ10933 that blends with the He I line.

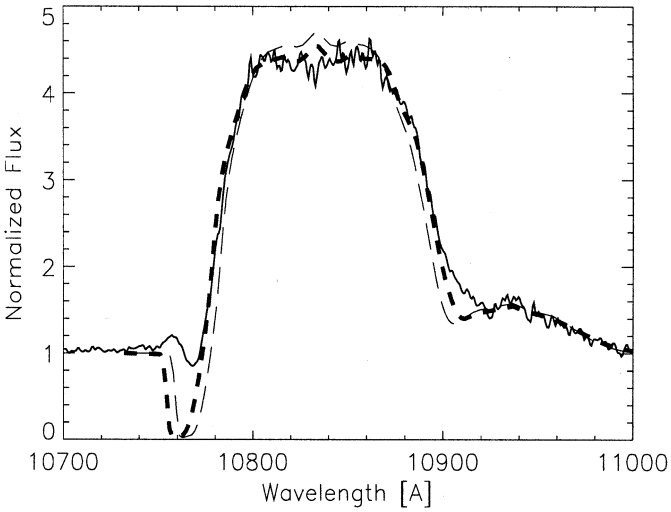

Fig. 2. Comparison of the observed He I λ10830 and He II (6-12) λ10933 line blend of HD 50896 (observation from Howarth & Schmutz 1992) with two synthetic profiles. The calculated profiles are based on velocity laws that have different terminal velocities. The short dashed profile results from a model with v_∞ = 2060 km s^{-1}; the long dashed profile denotes a model with v_∞ = 1930 km s^{-1}.

On the blue side of the He I profile the calculation predicts a pronounced P Cygni absorption that is not observed. Instead, there is only a weak absorption and at the blue end of the observed profile, there is a weak emission feature. P Cygni absorptions are predicted for other lines as well, e.g He I λ5876, but they are always observed to be much weaker, if present at all. As already shown by Hillier (1991b), clumping does not help to weaken the P Cygni absorption. No real explanation for this disagreement is at hand, except for the speculation that there is only low density material in front of the continuum emitting region. This hypothesis is at least in agreement with the interpretation of the depolarization that is observed across the emission lines. Schulte-Ladbeck et al. (1992) and Robert et al. (1992) conclude that the wind of HD 50896 is not spherically symmetric. Since the P Cygni absorptions are formed far from the photosphere it could be that on the direct line of sight to the continuum emitting region there is a void of material. The low density material would not only produce a much weaker absorption but its emission would also fill in absorption from the high density wind.

Because of the steep flanks of the almost box like shape of the profile of He I λ10830 the terminal velocity of the wind can be derived most accurately from the fit to this line. However, there are also other lines that could be used to determine the terminal wind velocity. The predicted widths of these lines are also in accordance with the observations (see below), confirming the derived velocity law in general and specifically, the value for the terminal velocity. In order to fit the observed He I λ10830 the synthetic profile has to be red-shifted by 100 km s^{-1}. The

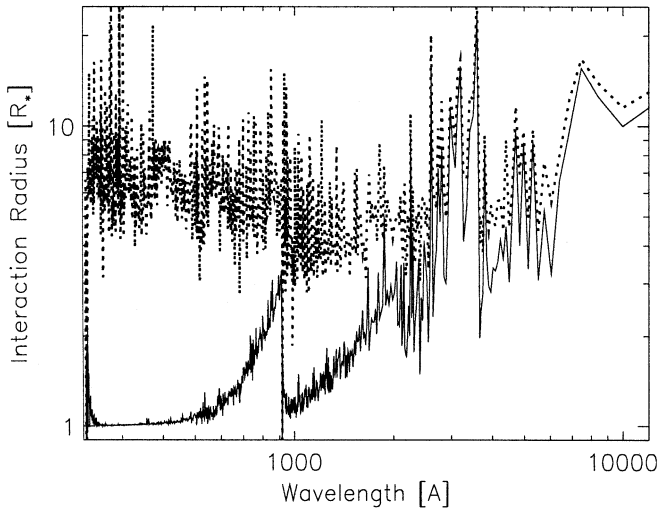

Fig. 3. Mean location where the photons are created as a function of wavelength (lower curve) and mean location where the photon interacted for the last time with the medium before they escaped from the atmosphere (upper, dotted line). In the optical and the UV wavelength range the last interaction is in most cases a scattering event. In the UV, many of the scatterings are due to interaction with spectral lines. This figure results from the formal solution of the radiation transfer with Monte Carlo simulation. The event statistic is low for the large wavelength end. However, in the UV many events are recorded (200,000) and the noise due to event statistics is not visible. The noisy appearance in the UV and even more pronounced, in the far UV is real. In this wavelength region the interaction with spectral lines is dominating the result. More than 20,000 spectral lines have been included in the simulation. At the wavelength locations of strong lines the photons are scattered even at large distances from the star.

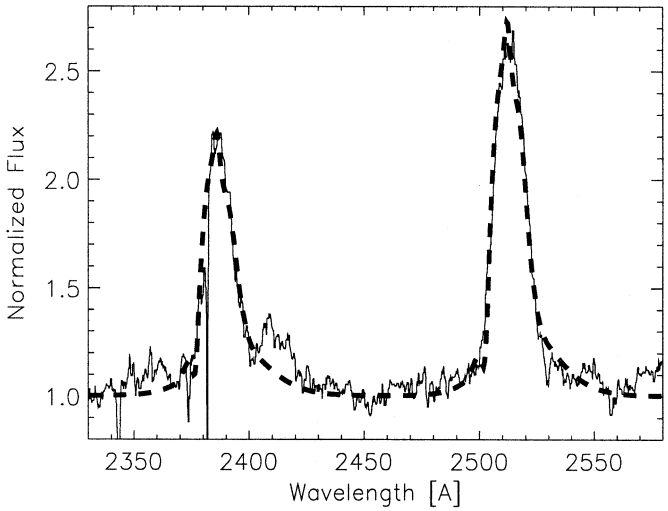

Fig. 4. Comparison of the observed He II (3-7) and (3-8) of HD 50896 (observation from Howarth & Philips 1986) with synthetic profiles. The widths of these profiles reflect the expansion velocity of the wind at the photosphere. The calculated profiles (dashed) are obtained with a velocity law that has 1100 km s^{-1} at the photosphere.

line shift can be determined to a precision of about 30 km s^{-1}. However, because the measured radial velocity depends on the predicted line profile, there is additional uncertainty contributed from the used velocity law. I estimate that the radial velocity of HD 50896 is accurate to about 50 km s^{-1}, thus $v_{\rm rad} = 100 \pm 50$ km s^{-1}. This value is smaller than the average value of $\approx$ 150 km s^{-1} determined by Ebbets (1979) but agrees well with his determination, considering the large spread of values from individual line profiles. Based on direct measurements, Ebbets (1979) and Robert et al. (1992) have determined very different radial velocities for different lines. It is therefore worth pointing out that the same shift of 100 km s^{-1} is needed in order to fit all other observed lines for which a synthetic profile is available.

3.2. The photospheric velocity

The expansion velocity of the wind at the photosphere is much more difficult to measure than the terminal velocity. The best lines to investigate the photospheric velocity are the weak transitions of the 3-n series in the UV. Willis (1982) has measured expansion velocities of 807 and 907 km s^{-1} from the profiles of He II $\lambda\lambda$2306, 2511. One advantage of these two lines is their weakness. This implies that the origin of these line photons is concentrated to the densest part of the observable the wind. In a monotonically accelerated wind this is the region just above the photosphere. The second advantage of these helium lines in the UV is that their wavelength that allows the deepest penetration of the Wolf-Rayet wind. Lines at longer wavelengths originate further out because the continuum opacity is larger. The wavelength dependence of the location of the photosphere is illustrated in Fig. 3. In this figure, the mean location is plotted where the photons are created and the mean location where the photons interact a last time with the medium. For optical and shorter wavelengths, this last interaction is almost always a scattering event. In most cases in the far UV, these scattering events are a line scattering, in the observable UV they are predominantly scatterings by electrons. The mean location of last interaction with the medium corresponds to the definition of the photosphere, i.e. $\tau = 2/3$. The mean location for creation of photons that escape the atmosphere corresponds to the definition of the thermalization optical depth $\tau_{\rm th} = 2/3$ (Mihalas 1978, p311). Most line photons originating in the region between the two locations undergo an electron scattering. The fraction of these photons that escape (many are scattered back) constitute the electron scattering wings. The main part of the line profile originates outside the location of last interaction and, in particular, weak lines are formed just above this location. As can be inferred from Fig. 3, the radius of the photosphere for $\lambda \approx 2500$ Å is $R_{\rm phot} \approx 5$ R$_*$. This radius corresponds, more or less, to the definition of $R_{2/3}$ given in the papers on analyses of Wolf-Rayet stars (Schmutz et al. 1989; Hamann et al. 1993, 1995). There is a small difference between the two definitions because $R_{2/3}$ is defined by the Rosseland mean optical depth and $R_{\rm phot}$ is defined here for the UV wavelength region. The Rosseland mean opacity is slightly larger than the opacity in the

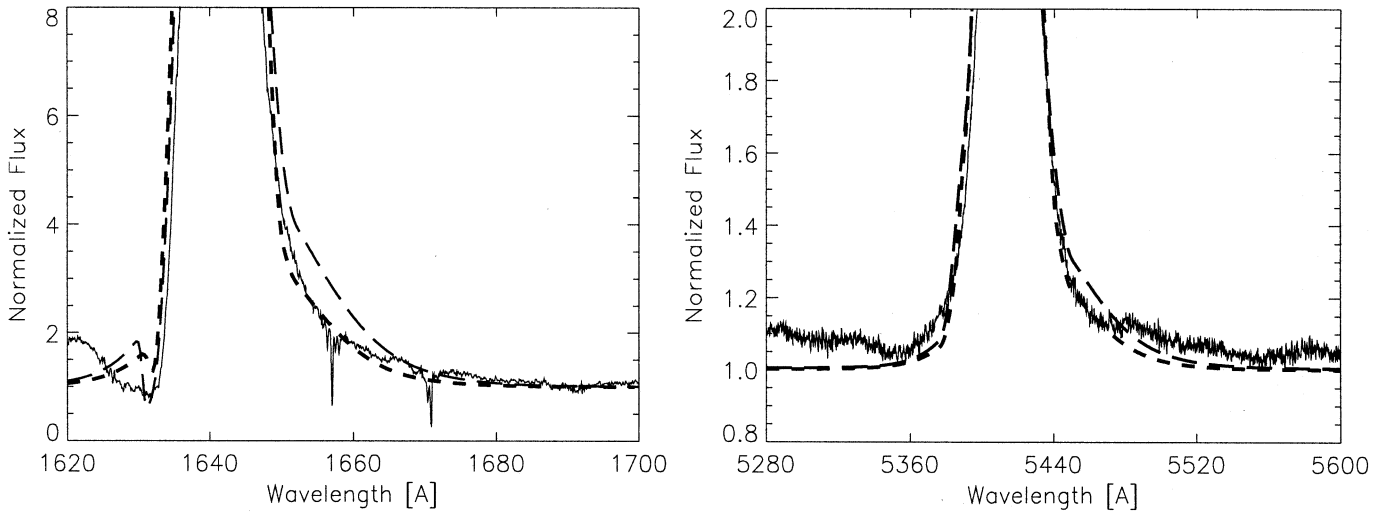

Fig. 5. Comparison of observed electron scattering wings from He II λ1640 and He II λ5411 of HD 50896 with synthetic profiles. The calculated profiles are based on mass loss rates that differ by 0.45 dex. Both profiles have the correct, i.e. observed, peak intensity.

UV and consequently, $R_{2/3}$ is a bit larger than $R_{\rm phot}$. In the case of the final model $R_{2/3}$ = 5.4 R_*.

In Fig. 4 the two lines He II $\lambda\lambda$2306, 2511 are compared with synthetic profiles calculated with a law that has an expansion velocity of $v_{\rm phot}$ = 1100 km s^{-1} at the photosphere. Most of the difficulty in deriving the expansion velocity at the photosphere comes from the fact that the form of these weak He II lines do not only depend on the photospheric expansion velocity but, to some extent, also on the faster velocities farther out in the wind. Therefore, when judging the agreement with observations more weight should be given to the width at the top of the profile than to the base. Inspection of different models has shown that the gradient of the velocity at the photosphere also plays a role. Thus, by fitting the observations the expansion velocity at the photosphere is not very well determined. At least some limits can be set. I find that profiles calculated with a photospheric expansion velocity of 900 km s^{-1} appear too narrow relative to the observed profiles. Thus, the precision with which I have determined the photospheric velocity is of the order of 200 km s^{-1}, thus, $v_{\rm phot}$ = 1100 $\pm$ 200 km s^{-1}.

3.3. The mass loss rate

The most important parameter that is determined from the line fits is the mass loss rate. The stellar luminosity results from this parameter and subsequently, in combination with the absolute magnitude, the radius and stellar temperature (see next subsection). In principle, the electron scattering wings allow the measurement of the mass loss rate. Fig. 5 illustrates how much the electron scattering wings change if the mass loss rate is varied by 0.45 dex. From this figure, it could be deduced that the mass loss rate can be determined to within about 0.1 dex. However, on the observational side there is considerable uncertainty in setting the continuum level. Almost all broad Wolf-Rayet lines are blended with other lines, and even if there is no other line evident there could still be some weak, flat-topped lines that form a pseudo continuum. On the theoretical side, there is also an unfortunate dependence on the velocity law. The mass loss rates shown in Fig. 5 are $\log(\dot{M}/(M_\odot/{\rm yr}))$ = -4.7 and -4.25, respectively. Thus, from this figure one would conclude that the mass loss rate of HD 50896 is $\log(\dot{M}/(M_\odot/{\rm yr}))$ = -4.7. However, the synthetic profiles in Fig. 5 are not calculated from the final model but from a velocity law that was obtained after one of the first solutions of the iteration. This law differs considerably from the finally adopted velocity law in that it has a larger velocity plateau at the photosphere. With the final law a mass loss rate of $\log(\dot{M}/(M_\odot/{\rm yr}))$ = -4.5 yielded the best fits to the electron scattering wings (Figs. 6 and 7). Thus, even if the difficulty of normalizing observed Wolf-Rayet spectra is not taken into account, there is an uncertainty of about a factor of two in the deduced mass loss rate.

3.4. The clumping factor and the photon loss factor

For a given velocity law and mass loss rate, it is straightforward to determine the remaining parameters, the clumping factor C and the photon loss factor f. The strength of the observed lines can be reproduced by adjusting the clumping factor and the observed He I to He II ratio by varying the photon loss factor. However, the procedure involves considerable computational effort. Each time these parameters are optimized, a mini grid of three or four models has to be calculated to interpolate the two parameters from a two-dimensional fit diagram. In Fig. 6 the line profiles of the final model are displayed. The line fit was optimized to reproduce the weak He II lines and He I λ10830. There is a systematic difference between the observed and calculated strong He II lines. The strong He II lines are always predicted to be stronger than the observed ones. In view of all the simplifying assumptions made for the model calculations, the disagreement is not alarming. For example, clumping is treated

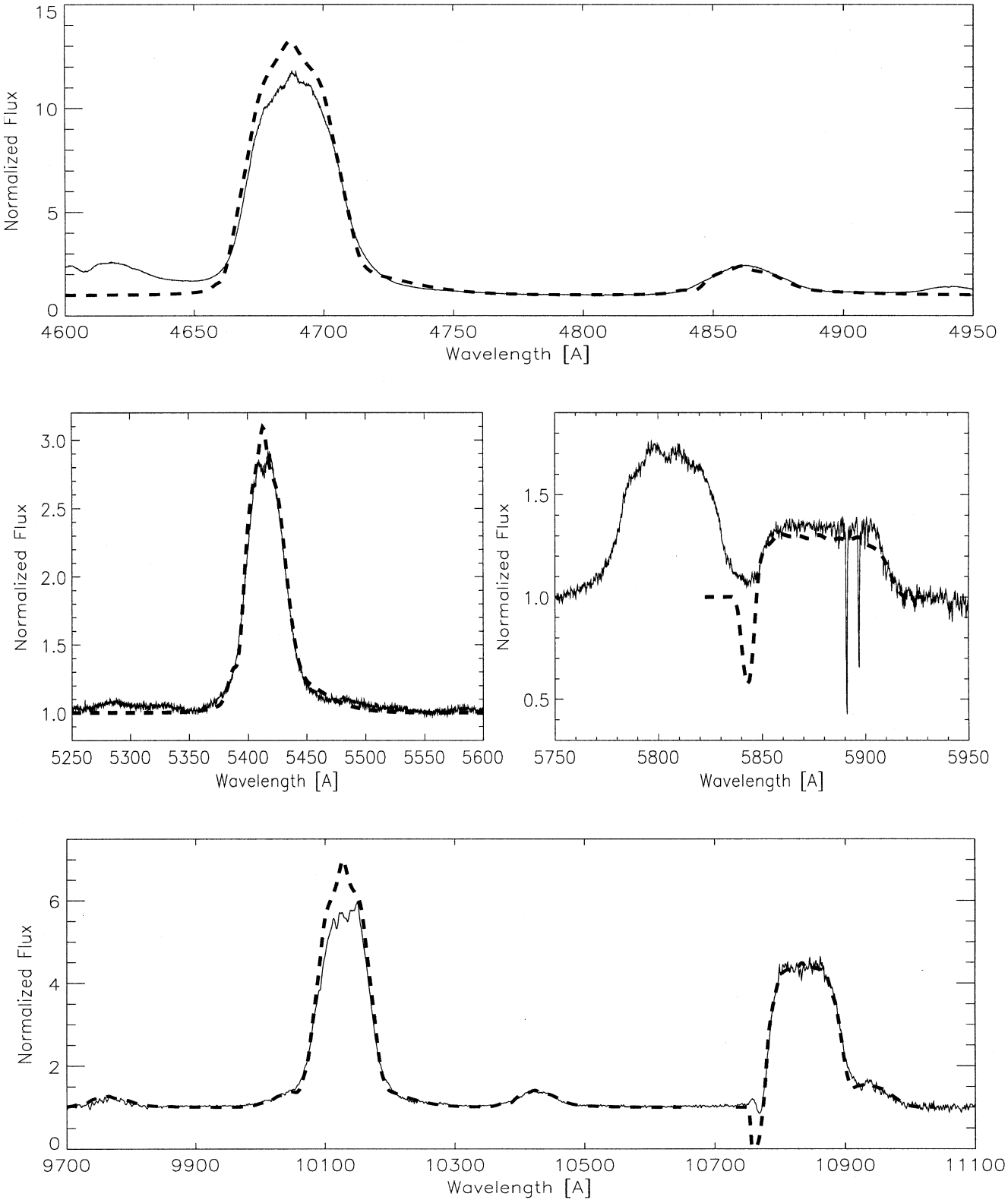

Fig. 6. Comparison of observed line profiles of HD 50896 with synthetic helium profiles (dashed). The profiles are calculated with the final model (see text). The displayed lines are: He II λ4686 and He II λ4859 (top panel), He II λ5411 (left middle), He I λ5876 (right middle), the He II (6-n) series He II $\lambda\lambda$9761, 10045, 10419, 10933, He II λ10123, and He I λ10830 (bottom panel) The near IR observation is from Howarth & Schmutz (1992) and the optical observations are made by the author.

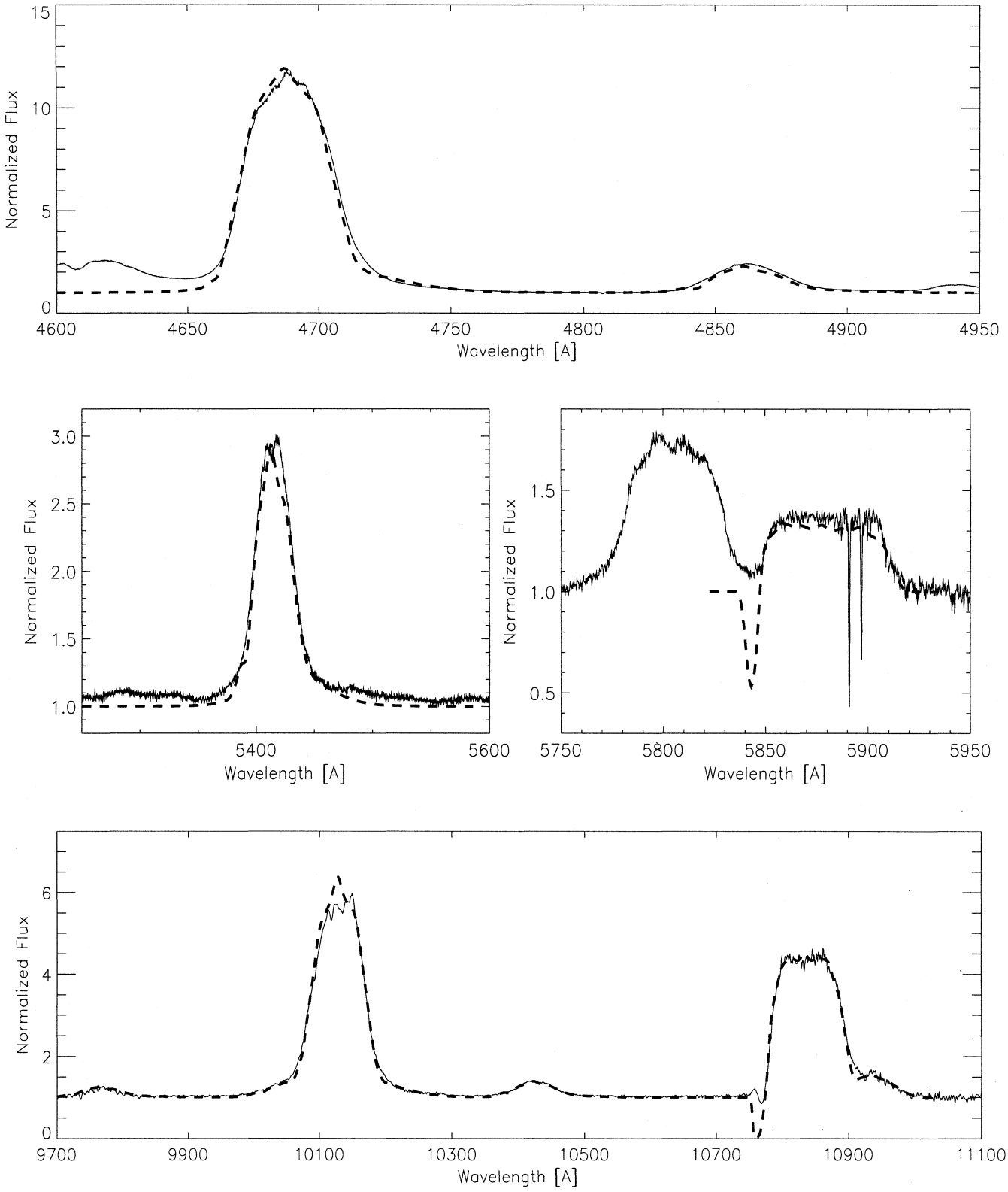

Fig. 7. As Fig. 6 but the synthetic profiles calculated with a model with clumping factor C = 3.8.

with only one factor. It could well be that at larger distances from the star this factor is smaller than at the photosphere. The model shown in Fig. 6 was calculated with a clumping factor of $C = 4.2$. In Fig. 7 a solution is shown with identical parameters as the model of Fig. 6 except for the clumping factor which was $C = 3.8$ and a slightly different photon loss factor. The agreement of the strong He II lines is better with this model than in Fig. 6 but weak He II lines, e.g. He II λ4859 (Fig. 7) or He II λ2511 (not shown), are predicted slightly too weak.

Since the two models differ only in marginally in their parameters and the line fits do not favor clearly one model over the other, I use the designation "final model" for both solutions.

The clumping factor implied by the line strengths can be compared with the ratio of the mass loss rate derived here using the electron scattering wings and the mass loss rate of HD 50896 as determined from its mm and cm radio emission. Assuming a homogeneous wind and adopting the newly determined wind terminal velocity, I derive from the observed cm radio flux (Hogg 1989) and mm flux (Leitherer and Robert 1991) a mass loss rate of of $\dot{M} = 9 \cdot 10^{-5}$ M$_\odot$yr^{-1}. Since free-free emission depends quadratically on the density, the ratio of the mass loss rate derived from the mm and cm emission to the mass loss rate derived here provides a linear measure of the clumping factor. The implied clumping factor is $C_{\rm radio} \approx 3$ in the mm and radio emitting region. This value is smaller then the factor $C_{\rm line} \approx 4$ as derived above. However, it is not clear whether the difference is really significant. At least, it supports the trend noted above that the clumping factor is largest close to the photosphere and becomes smaller with increasing distances from the star. Also compatible with this trend is the difference between the mass loss rates implied by the mm flux and the radio flux. Leitherer and Robert (1991) derived a larger mass loss rate from the mm flux than from the radio data.

A photon loss factor of $f = 1.0\,10^{-4}$ is used for the calculation shown in Fig. 6 ($C = 4.2$) and for the model of Fig. 7 ($C = 3.8$) the factor needed to fit the spectrum is $f = 1.2\,10^{-4}$. The clumping factor, as well as the photon loss parameter, turn out to be reasonable numbers within the expected range.

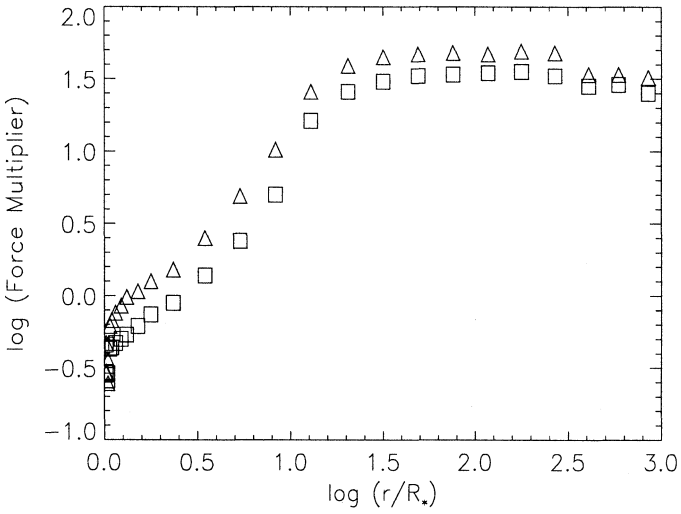

Fig. 8. The force multipliers from two identical models except for the mass loss rate. The comparison of the two models yields the CAK parameters $\alpha(r)$ and $k'(r)$ as function of the radius.

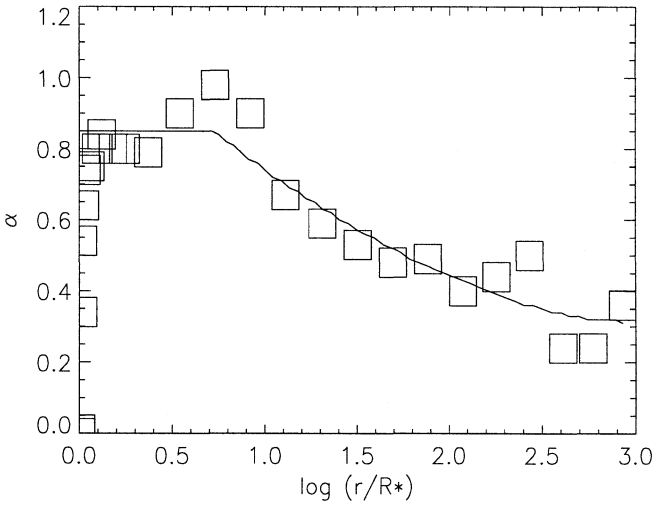

Fig. 9. The CAK parameter α as function of radius resulting from the two sets of force multipliers shown in Fig. 8. The line is a 2nd order polynomial fit to the α values truncated at $\alpha = 0.85$.

3.5. The hydrodynamical solution

3.5.1. Procedure

The iteration for a velocity law was started with a small grid composed of models with different $T_{\rm eff}$ and dM/dt, using a photon loss factor $f = 10^{-3}$, a clumping factor $C = 3$ and a slowly accelerating velocity law with $\beta = 2$. Then, with the method of Schmutz et al. (1989), the stellar parameters were determined that best fit the observed properties of HD 50896. With these stellar parameters, two identical atmosphere models are calculated except for the mass loss rates that differed by 0.15 dex. The formal solutions of the radiation transfer with the Monte Carlo code then yields the force multipliers. Fig. 8 shows an example of force multipliers as function of the radius. From the two sets of force multipliers the CAK parameter $\alpha(r)$ can be derived as a function of radius and subsequently, the parameter $k'(r)$ can be calculated. In Fig. 9 the parameter $\alpha(r)$ is shown as a function of radius. With the CAK parameter $\alpha(r)$ and $k'(r)$ known, the equation of motion is integrated inwards, starting at the outer model boundary. As a starting value, a terminal velocity of $v_\infty = 1820$ km s^{-1} was assumed. This value for v_∞ was obtained by Howarth & Schmutz (1992) by measuring the width of He I λ10830. The hydrodynamic solution is adjusted to reach a given value at the photosphere. The starting estimate for the photospheric velocity was adopted from the narrowest line widths measured by Willis (1982): $v_{\rm phot} = 900$ km s^{-1}. After each iteration these boundary values have been improved from the differences of the synthetic line widths to the observed ones

until convergence to the final values reported in Sects. 3.1 and 3.2.

The hydrodynamic solution yields the velocity as a function of radius. A characteristic for the solutions obtained for Wolf-Rayet winds is that the radiation force can only accelerate the wind from a certain distance outwards. Inside this point, the outward-directed forces are predicted to be insufficient and the wind solution is a coasting one, i.e. the wind decelerates outwards. Within the optically thick atmosphere, $\tau_R > 1$, I specify a velocity adopting $\beta = 0.5$. For the first iterations, the point where the hydrodynamic solution stopped was outside of $\tau_R = 1$. In these cases, I replaced the coasting wind solution with a flat but still outward accelerated law between $\tau_R = 1$ and the inner boundary of the hydrodynamic solution. Then, new atmosphere models are computed using the calculated velocity structure.

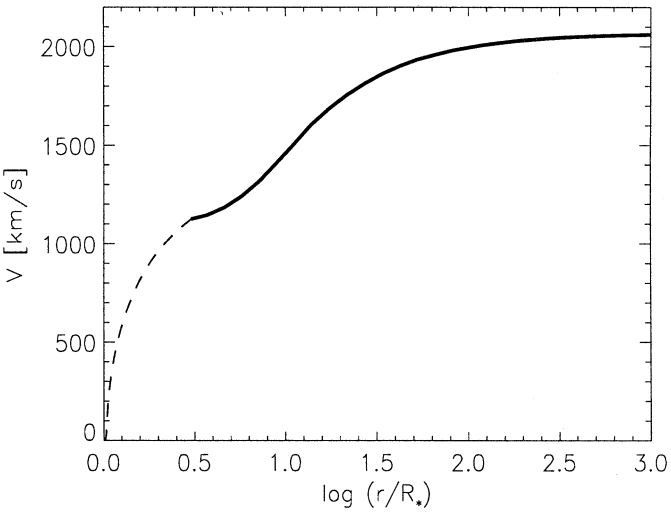

Fig. 10. The velocity structure of the final model. The hydrodynamically calculated velocity law is shown by the full drawn line, the assumed velocity law in the optically thick atmosphere is illustrated by the dashed line.

3.5.2. Convergence properties

The iteration for the velocity law turned out to be rather cumbersome. There are two reasons for a slow convergence. One reason is that it is not possible to calculate correct CAK parameters for certain locations in the atmosphere. In a Wolf-Rayet atmosphere the helium population is recombining in the wind from He^{2+} to He^{+}. Since the force multiplier is defined relative to the radiation force on electrons, and because the electron number per ion is changing by a factor two from one zone to the other, the force multiplier is also changing by a factor two within a relatively small distance.

The reason for ill-defined CAK parameters is that the two models do not have their recombination radius at the same location. The model with the higher mass loss rate recombines closer to the photosphere than the other model. I have tried to overcome this difficulty by using different photon loss factors for the two models to bring the two recombination regions in agreement. However, the result is not satisfactory. In Figs. 8 and 9 the effect of different locations of the recombination zone is still visible around radius $\log(r/R_*) \approx 1$, where α approaches values close to 1.

The second reason for a slow convergence of the velocity law is an incorrect description of the force multiplier by the CAK parameter α. According to theory (Castor et al. 1975) the parameter α describes the behavior of the force multiplier for changing density as well as for changing velocity gradient. As already explained, α is obtained by comparing two models with different mass loss rates. Thus, the parameter α is in fact determined for changing density but *including* the effects of a different density distribution on the radiation transfer solution. It turned out that in the extreme multi-scattering environment of a Wolf-Rayet atmosphere, the gradient-α is *different* from the density-α.

The gradient-α can be evaluated from two Monte Carlo simulations of the radiation transfer, with an artificially modified velocity gradient in one run. In this case the resulting gradient-α reflects the distribution of optically thin to optically thick lines (Abbott 1980). For the models discussed here the gradient-α is nearly independent of radius with $\alpha = 0.7 \pm 0.05$. A comparison of this value with the run of α in Fig. 9 shows that the two α's strongly differ.

Table 1. Derived luminosities for HD 50896 for given mass loss rate and boundary values for the velocity law.

$\log(\dot{M})$ [$M_\odot yr^{-1}$]	α	v_{phot} [km s^{-1}]	v_∞ [km s^{-1}]	$\log(L)$ [$L_\odot$]
-4.5	–[1)]	1100	2060	5.74
-4.5	0	900	2110	5.81
-4.5	0	1300	2010	5.66
-4.3	0.4	1100	2060	5.80

Note: 1) For the final model the radiation force is equal to the force required to support the velocity structure. For this model the CAK parameters are irrelevant.

The practical implication of the ill defined α parameter is that the predicted force multiplier using α and k' is incorrect. For example, in subsequent iterations I found sufficient radiation force to support the wind structure in zones where previously it was not possible to solve the equation of motion. After the overall shape of the velocity law converges and the mass loss rate is determined I find better predictions for the next velocity solution if I use $\alpha = 0$ instead of the density-$\alpha(r)$. So far, I have not found a procedure to improve the convergence of the iteration of the velocity structure.

3.6. The final velocity law

Fortunately, once a consistent solution is found, the CAK parameters are no longer important, since these parameters are only used to predict the force for other densities and gradients than those of the last solution. The only test that matters is *whether the calculated radiation force agrees with the force required to*

Table 2. Ionization structure of the model for HD 50896.

depth point	He	C	N	O	Ne	Na	Mg	Al	Si	P	S	Cl	Ar	K	Ca	Cr	Mn	Fe	Ni
1	III	V	VI	VII	III	VII	VII	VII	VII	VII	VII	VIII	IX	X	X	IX	IX	IX	IX
5	III	V	VI	VII	VII	VII	VI	VI	VI	VI	VII	VIII	IX	IX	IX	IX	VIII	IX	IX
10	III	V	VI	VII	VII	VI	VI	VI	VI	VI	VII	VIII	IX	IX	IX	VIII	VIII	IX	VIII
11	III	V	VI	VII	VI	VI	VI	VI	VI	VI	VII	VIII	IX	IX	IX	VIII	VIII	VIII	VIII
12	III	V	VI	VII	VI	VI	VI	V	V	VI	VII	VIII	VIII	VIII	VIII	VII	VIII	VIII	VIII
13	III	V	VI	VI	VI	V	V	V	V	VI	VII	VIII	VIII	VIII	VIII	VII	VIII	VIII	VIII
14	III	V	VI	VI	V	V	V	V	V	VI	VII	VIII	VII	VII	VII	VII	VII	VII	VII
15	III	V	V	V	V	V	IV	IV	V	VI	VII	VII	VII	VI	VI	VII	VII	VI	VI
16	III	V	V	V	IV	IV	IV	IV	V	VI	VI	VI	VI	VI	V	VI	VI	VI	VI
17	III	V	IV	IV	IV	III	III	IV	V	VI	V	V	V	V	V	V	V	V	V
18	III	IV	IV	IV	III	III	III	IV	V	V	V	V	IV	IV	IV	V	V	V	V
19	II	IV	IV	III	III	III	III	IV	V	V	V	V	IV	IV	IV	V	V	IV	IV
20	II	IV	IV	III	III	III	III	IV	V	V	V	V	IV	IV	IV	V	V	IV	IV
21	II	IV	IV	III	III	III	III	IV	V	V	V	V	IV	IV	IV	V	V	IV	IV
22	II	IV	IV	III	III	III	III	IV	V	V	V	V	IV	IV	IV	V	V	IV	IV
23	II	IV	IV	III	III	III	III	IV	V	V	V	IV	IV	IV	IV	V	V	IV	IV
24	II	IV	IV	III	III	III	III	IV	V	IV	IV	IV	IV	IV	IV	V	V	IV	IV
25	II	IV	IV	III	III	III	III	IV	V	IV	IV	IV	IV	IV	IV	V	V	IV	IV
26	II	III	IV	III	III	III	III	IV	IV	IV	IV	IV	IV	IV	IV	V	IV	IV	IV
27	II	III	III	III	III	III	III	IV	IV	IV	IV	IV	IV	IV	IV	IV	IV	IV	IV

Note: The location of the entries within the atmosphere can be identified in Fig. 11. There, the calculated force multipliers (dots) correspond to the entries given in this table. The last dot shown in Fig. 11 is at $\log(r) = 2.83$ and corresponds to entry #27. The calculated ionization structure of helium is illustrated in Fig. 12 and that of iron in Fig. 13.

support the velocity structure of the model. The final velocity law is shown in Fig. 10. The outer part can be approximated with $\beta = 3$ if the model R_* is used as the reference radius. For $r < 10$ R$_*$ the velocity law turns over to a flat structure around the photosphere with an expansion velocity of about half the terminal velocity. In Table 1 the input parameters for the hydrodynamical solution, $v_{\rm phot}$, v_∞, and $\dot{M}$, are listed together with the resulting luminosity, that is needed to solve the hydrodynamical equation. The comparison of the calculated force with the force needed to support the velocity structure is shown in Fig. 11. The small deviations of the actual and required force is negligible since for a new predicted velocity law the velocities differ not more than a few 10 km s^{-1} from the present solution, and such small changes of the velocity law are no longer visible in the line profiles. Fig. 11 shows that there is a strong increase of the force multiplier around $r \approx 10$ R$_*$. As can be inferred from the location of the step of the gravity term, this increase coincides with the recombination zone of helium. This region is also the most important part for the acceleration of the wind. From $r = 9$ to $r = 25$ R$_*$ the wind is accelerated from 1400 km s^{-1} to 1800 km s^{-1}. This is 40% of the acceleration in the optically thin atmosphere. At larger distances, where the force multiplier has its maximum, there is only an acceleration of another 30%. Despite the large force multiplier, this region is already too far from the star to be of prime importance for the wind acceleration. Another 30% of the wind acceleration is contributed from the region where helium is fully ionized. When inspecting the ionization structure of the metals in the atmosphere, which is given in Table 2 and illustrated for helium and iron in Figs. 12 and 13, it is seen that the 4 and 5 times ionized metals of the iron group elements are the most important ionization stages for the acceleration. Since strong radiation pressure on spectral lines also implies a strong blanketing effect, the emergent spectrum is blanketed predominantly by Fe V and Fe VI lines. Fig. 14 illustrates this blanketing effect. The calculation predicts lower ionization stages to be at larger radii and thus, to be in regions with higher expansion velocities. This trend is confirmed by observations (Willis 1982; Niedzielski 1994; Dalton et al. 1995).

3.7. The luminosity

In Table 1 there are three other hydrodynamical solutions that allow an estimation of the precision of the luminosity determination. Since these solutions do not result from a consistent model, it matters what CAK parameters are used. As listed, I have assumed $\alpha = 0$ for velocity laws that differ mainly in their gradient from the present solution and $\alpha = 0.4$ for the solution with a change of the density. From these hydrodynamical results the inferred luminosity of HD 50896 is $\log(L/{\rm L}_\odot) = 5.74 \pm 0.1$. The mass implied by this luminosity is $M = 20 \pm 3$ M$_\odot$ using the mass-luminosity relation for Wolf-Rayet stars (Schaerer & Maeder 1992). Imposing the constraint that the model reproduces the observed visual magnitude $M_v = -4.6$ (Howarth & Schmutz 1995), I find that $R_* = 3.5$ R$_\odot$ and, since $R_{\rm phot} = 5$ R$_*$ (Fig. 3), a photospheric radius for HD 50896 of $R_{\rm phot} = 18$ R$_\odot$.

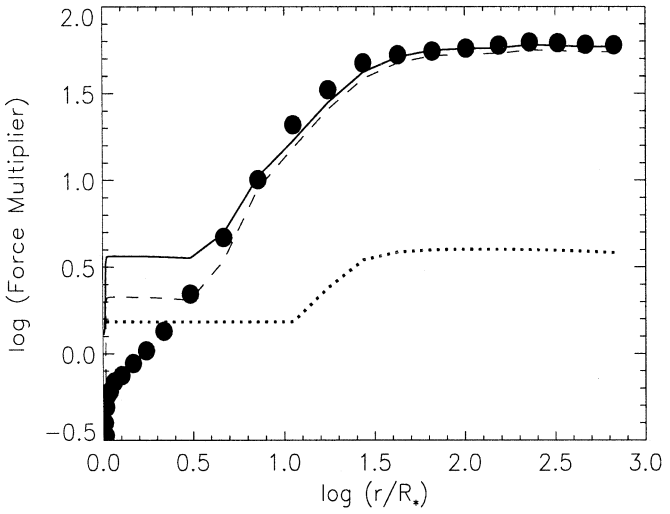

Fig. 11. Comparison of the calculated force multiplier (filled dots) with the factors needed to drive the wind (full drawn line). The dashed line illustrates the contribution by the kinematic term, i.e. the multiplier required for the acceleration of the wind without inclusion of gravitation, and the dotted line gives the factors needed to support the material against gravity. The unit of the force multiplier is the radiation force on electrons. Since this unit depends on the electron scattering opacity, there is a reduction of the electron force when helium recombines from He^{2+} to He^{+}. Therefore, the step in the line denoting the gravitational term occurs at the recombination zone.

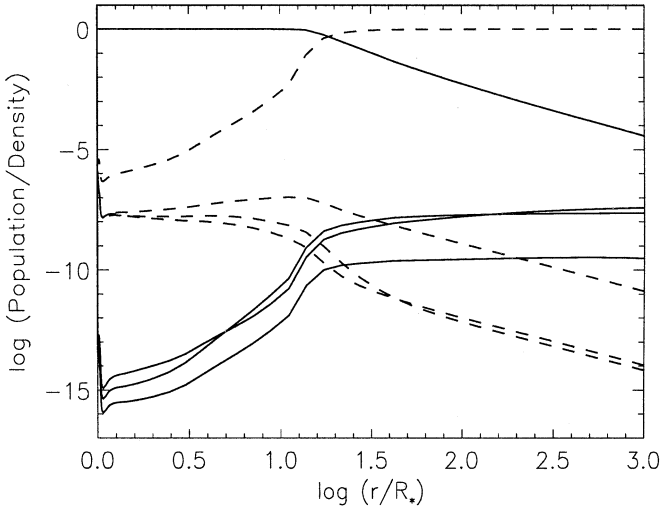

Fig. 12. The ionization structure of helium from the final model. The full drawn lines mark the populations of the three lowest energy terms of He^0 and the population of He^{2+}. The dashed lines denote the populations of the first four main quantum numbers of He^{+}.

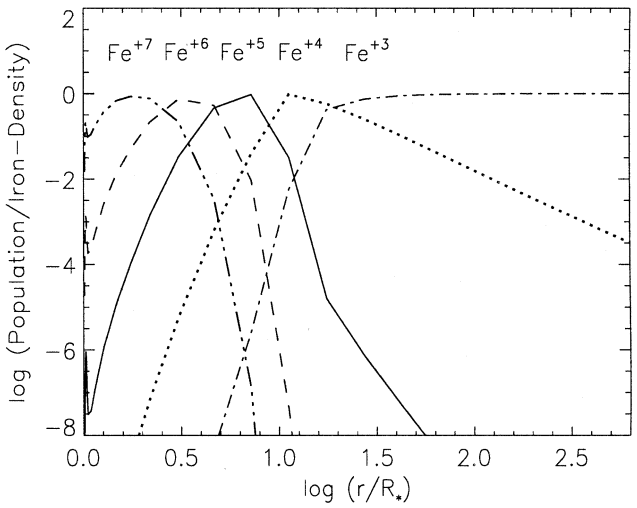

Fig. 13. The ionization structure of iron from the final model. The ionization stages are marked at the radial position where a given ion is the dominant stage..

The corresponding effective temperatures are $T_* = T_{\rm eff}(R_*)$ = 84 kK and $T_{2/3} = T_{\rm eff}(R_{\rm phot})$ = 37 kK. It is completely justified to call T_* an *effective* temperature since the photons that comprise most of the emitted energy (the far UV photons) are created at R_* (see Fig. 3). However, as already pointed out, the determination of R_* is arbitrary and therefore, too much weight should not be given to this value of T_*.

The static stellar interior models of Schaerer & Maeder (1992) also predict a radius $R_{\rm evol}$ for a Wolf-Rayet star as a function of its mass. In our case this is $R_{\rm evol}$ = 1.25 $R_\odot$. It might be considered as the location where the stellar wind has its origin. However, this location is buried at high optical depth. The corresponding effective temperature would no longer be characteristic for the energy distribution since such a small radius is inside the formation depth of all photons. The temperature T_* as determined here has the advantage of at least describing reasonably the form of the emergent spectrum. If the small radius of a stellar interior model is used as reference for a β-law then the calculated velocity law (Fig. 10) in the optically thin part of the atmosphere can be approximated using β = 8.4.

4. Calculation of the photon loss factor

In the fitting procedure (cf. Sect. 2.2.3) the photon loss factor has been treated as a free parameter. It was found (Sect. 3.4) that a value of $f \approx 10^{-4}$ is needed in order to reproduce the observed ionization structure.

Lucy et al. (1991) have shown that Na I transitions in the wing of the optically very thick Mg I λ2853 line in SN 1987A have a pronounced effect on the population of the upper magnesium level. Here, we propose a similar process for the He II Lyα line. Based on the level populations of the final model the photon loss factor can be numerically evaluated with the formulation derived in the appendix (Eq. A5 or Eq. A10).

In Fig. 15 the line opacities are displayed for a location in the atmosphere ($\log r$ = 0.9, between point 16 and 17 of Table 2) where photon loss becomes important for the ionization structure. The calculation of the photon loss factor depends on line width, i.e. the factor is a function of broadening. In Fig. 15 the

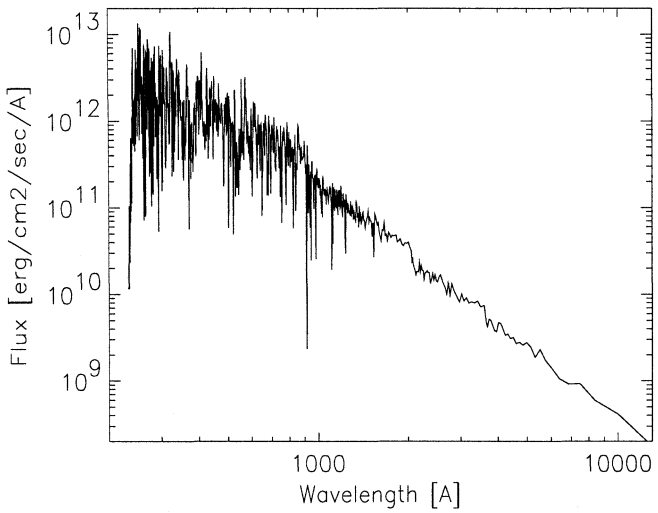

Fig. 14. Emergent spectrum calculated with Monte Carlo simulation. The event statistic is proportional to the emergent energy. Thus the wiggles at long wavelengths are due to simulation noise. But the noisy appearance in the UV is real. There, the spectrum is blanketed by the effect of more than 20,000 lines.

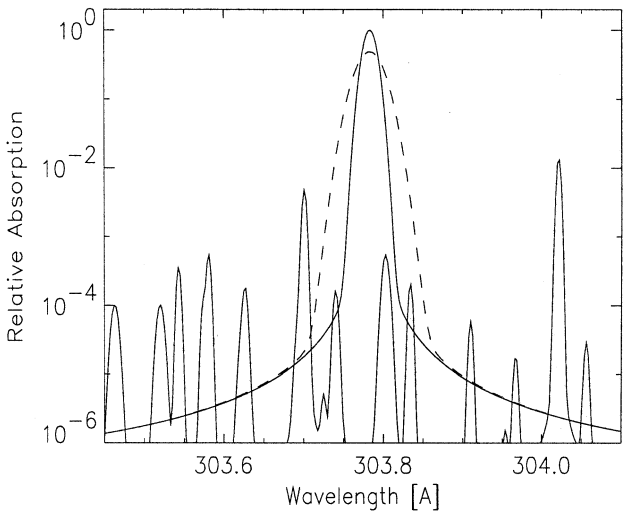

Fig. 15. Relative opacities of helium and metal lines at $\log r = 0.9$ (between point 16 and 17 in Table 2). The full lines give the profiles for temperature broadening only, whereas the dashed line indicates the shape when 20 km s^{-1} turbulence is added. The metal lines close to the rest wavelength of He II λ303.78 are Ca V λ303.74, Fe VI $\lambda\lambda$303.70, 303.80, 303.83, Ni V $\lambda\lambda$303.73, 303.91, and O III λ303.80.

full lines denote the line profiles for the case of thermal broadening only. The dashed line gives the helium line profile with $v_{\rm turb} = 20$ km s^{-1}. Additional turbulent broadening increases the influence of lines with larger wavelength separation from the helium line.

Fig. 16 shows the contributions by individual transitions to the capture factor (cf. Eq. A8). Around $\log r \approx 1$, helium recombines and the ionization of the metals also changes to lower stages (cf. Figs. 12 and 13).

The depth dependence of the photon loss factor (Eq. A10) is shown in Fig. 17 for three assumptions of turbulent broadening. At $\log r \approx 1$, the photon loss factor is of the order $f^* \approx 10^{-4}$, in excellent agreement with the factor determined empirically. In the inner part $\log r \lesssim 1$, the photon loss factor is close to the capture factor, i.e. $\bar{J}^* > S^{\rm mi}$ (cf. Eq. A10). This is advantageous for the reliability of the calculated value because the capture factor depends in first approximation only on the wavelength positions of the metal lines (Eq. A12).

Outside the He^{++} recombination zone, where helium is dominantly in the form of He$^+$, the calculated photon loss is negative, i.e. there is a gain of photons provided by the metal transitions. This is because the helium line radiation field $\bar{J}^*$ (Eq. A3) is smaller than the source function of the metals. It is unclear whether this result is robust. The non-LTE level populations of the metals are calculated with an approximative treatment that is based on the continuum radiation field (cf. Schaerer & Schmutz 1994). Thus, an interaction with the helium line is not taken into account. It is possible that a more realistic treatment yields a positive factor also for the outer part.

It is important to note that the inclusion of photon loss for the helium transition has only significant consequences for the region where helium recombines (cf. Sect. 2.1.2). Further in as

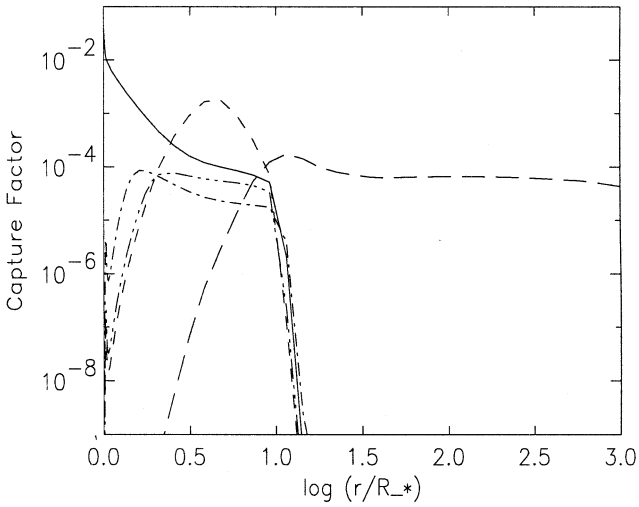

Fig. 16. Contributions to the capture factor $f^{\rm cap}$ (Eq. A8) by the lines Ca V λ303.74 (full drawn line), Fe VI λ303.80 (dashed), Fe VI λ303.70 (dash-dotted), Fe VI λ303.83 (dash-dot-dot-dot), and O III λ303.80 (long dashes).

well as further out, the rate equations are not sensitive to a small perturbation of the line radiation field of the He II Lyα line.

The process proposed for the photon loss of the helium line is a Bowen-type fluorescence mechanism for the excited metal transitions. In principle, there should be observable lines testifying for the proposed process. Unfortunately, the continuum radiation field is comparable in intensity with that of the helium line intensity and therefore, there is also efficient continuum fluorescence producing numerous Fe V and Fe VI lines in the

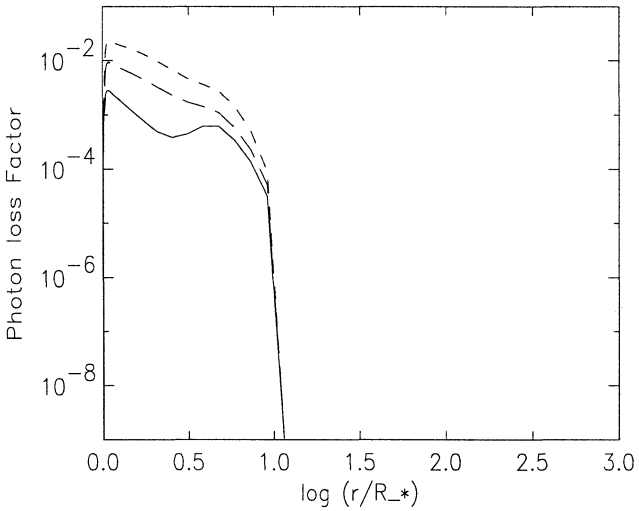

Fig. 17. Photon loss factors f^* (Eq. A10) for three assumptions of turbulent broadening: $v_{\rm turb}$ = 0 km s^{-1} (full drawn line), $v_{\rm turb}$ = 10 km s^{-1} (long dashes), and $v_{\rm turb}$ = 20 km s^{-1} (short dashes). The photon loss factors are negative for $\log r > 1$.

Table 3. Comparison of the stellar parameters of HD 50896 derived in this work with earlier determinations

Paper	$\log(\dot{M})$ [M$_\odot$yr^{-1}]	v_∞ [km s^{-1}]	$\log(L)$ [L$_\odot$]	$\dot{M}v_\infty/(L/c)$
this work	-4.5[1]	2060	5.74	6.0
H87	-4.3	1625	5.0	40.
HSW88	-4.0	1700	5.4	33.
SHW89	-4.0	1700	5.4	33.
HS92	-4.0	1820	5.1	71.
HKW93	-4.1	1700	5.2	42.
PAC93	-4.1	1720	5.3	34.
LA93	-4.7	2500[2]	5.46[2]	8.8

Notes: The references are: H87 Hillier (1987); HSW88 Hamann et al. (1988); SHW89 Schmutz et al. (1989); HS92 Howarth & Schmutz (1992); HKW93 Hamann et al. (1993); PAC93 Crowther (1993); LA93 Lucy & Abbott (1993)

1) This mass loss rate is derived together with a clumping factor of C = 4

2) LA only derive the mass loss rate, v_∞ and L are adopted from the literature.

observable UV (Koenigsberger & Auer 1985, Nugis & Sapar 1985, Hillier 1991a). In the spectrum of HD 50896 there are emission features at the wavelengths of transitions from upper Fe VI levels possibly excited by the helium line. However, there are also hundreds of other iron lines and blend effects that make it impossible to single out a particular transition.

So far no O III Bowen emission lines (Bowen 1935) have been identified in Wolf-Rayet spectra. However, there is now a direct proof from far UV observations that O III λ303.80 is excited by the He Lyα line in a B star atmosphere (Cassinelli et al. 1996).

The Ca V λ303.74 line excites 3d$''$ ^{1}F^0 which decays in most cases to 3p ^{1}D. This level is connected to the ground state via the resonance intercombination transition Ca V λ5309.2. In the spectrum of HD 50896 there is a weak flat toped feature at this wavelength with a peak intensity of $\approx$ 5% of the continuum level. It might be possible to test the proposed photon loss mechanism with detailed non-LTE calculations of the involved calcium levels.

5. Discussion

A comparison of the stellar parameters derived in this work with previously determined stellar parameters reveals that in the present work, the Wolf-Rayet momentum problem is solved with two contributions of equal magnitude. As can be seen in Table 3, the assumption of clumping allowed a reduction of the mass loss rate by about a factor of 3. An increase in the luminosity contributes another factor of 3 to the reduction the momentum ratio $\dot{M}v_\infty/(L/c)$. Interestingly, an analysis of the ring nebula S308 that surrounds HD 50896 yielded a luminosity of $\log(L/{\rm L}_\odot)$ = 5.6, for the Wolf-Rayet star (Esteban et al. 1993). Although the uncertainty of their determination does not allow any firm conclusion, their result supports the luminosity derived here. Thus, *the main ingredient that allows the calculation of a Wolf-Rayet wind is not a method that yields a huge momentum ratio, but a reduction of the momentum ratio to a more "normal" value.* With the new model the momentum transfer efficiency for HD 50896 should be 6 times the single scattering limit. Half of this value is provided by the present model in the optically thin part of the atmosphere.

Increasing the luminosity and lowering the mass loss rate have a direct consequence for the mass loss dependence on the mass. Such a relation is important for evolutionary calculation in the Wolf-Rayet phase. Langer (1989) has advocated $\dot{M}$ = (0.6 – 1.0) $10^{-7}(M_{\rm WR}/{\rm M}_\odot)^{2.5}$ M$_\odot$yr^{-1}. With this relation, a star of 20 M$_\odot$ should have a mass loss rate of $(1-1.8)\,10^{-4}$ M$_\odot$yr^{-1}. In fact, this number agrees with the mass loss rate derived when no clumping effects are taken into account (cf. Table 3). However, when compared with the mass loss rate derived here, Langer's formula yields a rate that is about a factor 3 too large. There is no other Wolf-Rayet star for which the mass loss rate has been determined using the electron scattering wings. But for V444 Cyg there is a mass loss rate derived from the change of its orbital period. Antokhin et al. (1995) have found a loss rate of 7 10^{-6} M$_\odot$yr^{-1}. The mass of the Wolf-Rayet object in this binary is 9.3 M$_\odot$ (Marchenko et al. 1994). Combining these two results yields a mass loss dependence on the mass with the power 2 instead of 2.5 and the relation reads

$$\frac{\dot{M}}{{\rm M}_\odot{\rm yr}^{-1}} = 8\,10^{-8}\left(\frac{M_{\rm WR}}{{\rm M}_\odot}\right)^2 . \quad (1)$$

Since there are only two values it is difficult to estimate an uncertainty of the newly proposed relation, especially since the two mass – mass loss pairs are derived with methods that completely

differ. Formally, an intrinsic uncertainty may be derived by using uncertainties of the four values. In Sect. 3.3 I have estimated that the mass loss rate of HD 50896 is uncertain to about a factor 2. This contribution alone could raise the power to 2.5. The uncertainty of the mass loss rate of V444 Cyg may be estimated by comparing the values derived by different groups: Underhill et al. (1990) found a rate of $5.6\,10^{-6}$ $M_\odot yr^{-1}$ and Eaton & Henry (1994) determined $8.1\,10^{-6}$ $M_\odot yr^{-1}$. If the two uncertainties for the mass loss rates are combined, one finds that the dependence on the mass could have a power as large as 3. Thus, the mass loss law is not discrepant from the power determined by Langer (1989). The real difference with Langer's formula is only that the constant factor is found to be smaller due to the effect of clumping. If Langer's power 2.5 is adapted, then this constant is $2.4\,10^{-8}$ based on the average of the two loss rates.

There is a third method to determine mass loss rates that does not depend on the clumping factor in the wind: polarization variability of binary Wolf-Rayet stars. It is noteworthy that both mass – mass loss pairs, the mass loss rate and mass determined for HD 50896 in this paper and the values for V444 Cyg, agree remarkably well with the values derived from the polarization variability method (St.-Louis et al. 1988). A formula with a smaller factor than proposed by Langer (1989) should therefore be considered in future investigations of the ratio of WN to WC stars. Whether or not a different power to the mass than Langer's value should be considered cannot be decided with the present available data.

An important difference between the hydrodynamic solution presented here and the solution of LA is that here, only the acceleration in the optically thin part is explained, starting from a photospheric expansion velocity $v_{\rm phot}$, whereas LA solved for the force required to accelerate the wind from zero velocity to the terminal velocity. However, as pointed out by Springmann (1994), LA provide too much force in the outer part of the wind and not enough in the inner part. Thus, in fact, if LA attempted a velocity structure which is consistent with the radial distribution of the radiation force, then they would have found a solution where most of the acceleration takes place in the outer wind. It is noteworthy that Springmann (1994; see also Friend & Castor 1983; Gayley & Owocki 1995) predicted quantitatively such a shape for the velocity law based on simple assumptions regarding the radiation force.

In principle, it would be possible to calculate a solution with the method of the presented here where the whole acceleration from subsonic velocities to the terminal velocity takes place in the optically thin part and is provided by the radiation force. As demonstrated in Table 1, the inner boundary condition, $v_{\rm phot} \approx 1/2\, v_\infty$, is not a result of missing force in the present hydrodynamic calculation – the radiation force can be increased by simply increasing the luminosity. Instead, the existence of a fast photospheric velocity is imposed by the observed line profiles. The line fits exclude a solution where an acceleration from subsonic velocities takes place in the optically thin atmosphere. The comparison of the synthetic line profiles with the observed ones imposes a wind with a velocity of about half the terminal velocity at the photosphere. It is not only the He II lines shown in Fig. 4 but also many other lines such as He II $\lambda\lambda$9761, 10045, 10419, 10933 (Figs. 6 and 7), which are weak but broad, that testify to a fast expansion at the photosphere.

With the luminosity and outer velocity structure imposed by the observed spectrum, it turns out that the present model does not yield enough force to drive the wind in the inner, optically thick part. Although it cannot be excluded that the wind's creation and first acceleration is by some other mechanism I still argue that it is also due to radiation pressure. I suspect that the present calculations do not correctly evaluate the radiation pressure in the highly ionized regions and that the missing force is probably located below the photosphere. Thus, from an inspection of Table 2, I identify six and seven times ionized metals of the iron group as the most probable candidates, for which in the present line list a significant number of transitions are missing. This conclusion is supported by a comparison of OPAL opacities (Iglesias et al. 1992) with Rosseland opacities that are evaluated with models similar to that of the present work (Schaerer et al. 1995). In the outer atmosphere the opacity from our expanding line blanketed non-LTE atmosphere is higher than the OPAL opacities, as expected for an expanding atmosphere, whereas in the inner part the OPAL opacities are a factor of two larger, indicating that the present evaluation of the line force is deficient in the inner part.

A terminal wind velocity of $v_\infty = 2060$ km s^{-1} for HD 50896 is definitely higher than previous determinations. Using line fits based on model atmospheres Hillier (1987) found 1625 km s^{-1} and Hamann et al. (1988) determined 1700 km s^{-1}. The terminal velocity derived here is also higher than those inferred from measurements of line widths. Prinja et al. (1990) determined 1720 km s^{-1} and Howarth & Schmutz (1992) found 1820 km s^{-1}. This comparison clearly illustrates the difficulty in measuring the terminal velocity more accurately than a few 100 km s^{-1}.

The reason for the underestimation of the terminal velocity by those two papers that used model atmospheres becomes clear when their velocity law is compared with the velocity law calculated in the present work. In Fig. 18 the present velocity law is compared with that used by Hamann et al. (1988). It can be seen that the velocity law with $\beta = 1$ used by Hamann et al. (1988) approximates more or less the expansion velocities in the region where most of the line flux emerges, i.e. between $x = R_*/r = 0.2$ and 0.05. Therefore, Hamann et al. (1988) could reproduce satisfactorily most of the observed line profiles, but they failed to fit the width of He I λ10830 (see Fig. 2 of Hamann et al. 1988) – a line that reflects the fasted velocities – since their velocity law does not reach the correct terminal velocity. From the larger expansion velocities inferred from the UV lines Hillier (1987) predicted that the He I λ10830 line would show a broader width and he concluded that the correct terminal velocity of the wind is larger than the value of his model.

Regarding the quality of line profile fits, the hydrodynamically calculated velocity law has yielded a remarkable improvement. The agreement in general shape of the synthetic profile of He I λ10830 is of such good quality that it strongly supports the correctness of the hydrodynamically calculated velocity law of

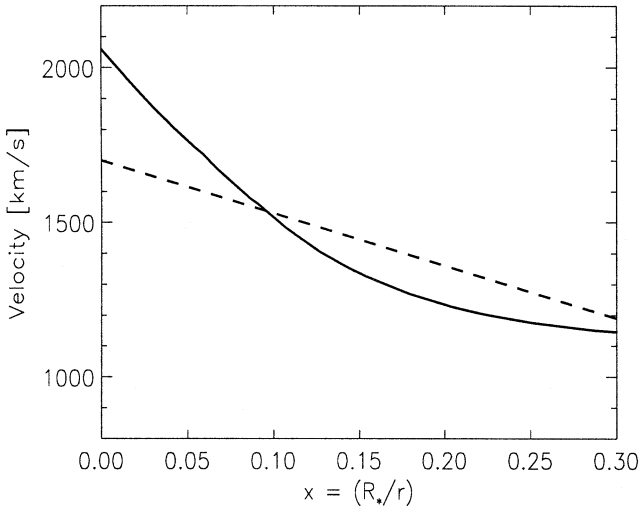

Fig. 18. The hydrodynamically calculated velocity structure (full drawn line) for HD 50896 compared with the β-law (β = 1) used in the analysis of Hamann et al. (1988) (dashed line). The photospheric radius is at x = 0.2 (see Fig. 3).

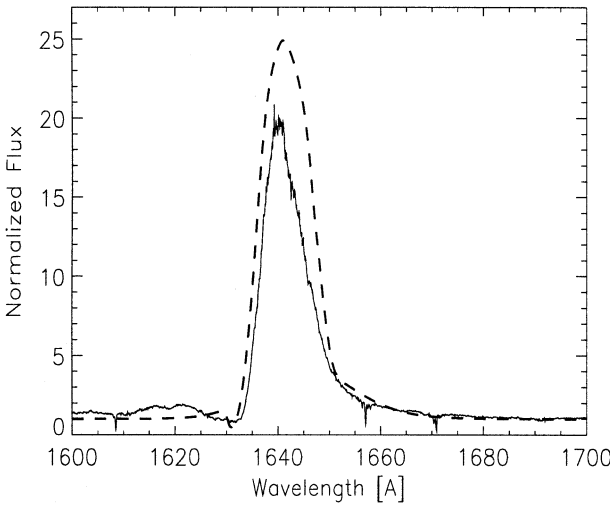

Fig. 19. Comparison of the observed He II λ1640 of HD 50896 (observation from Howarth & Philips 1986) with the calculated profile.

the outer atmosphere. The fits to all other line profiles are also satisfactory with one exception. As illustrated in Fig. 19 the line He II λ1640 is not only predicted too strong but the synthetic profile does also not fit the shape of the observed line. As mentioned in Sect. 3.4, the fact that some lines turn out to be too strong could be explained by a non-constant clumping factor in a real atmosphere. However, there is no easy explanation for the rather rounded shape of the synthetic profile that is in contradiction with the triangular shape of the observed line. An inspection of Fig. 3 reveals that this line is unique in the sense that the continuum formed at 1640 Å is formed at the largest depth. The continuum photons at this wavelength are created at r = 2 R$_*$. Thus, part of this line is formed in the region where I have assumed the β-law for the velocity structure. The disagreement between the observed and calculated profiles could indicate that the adopted velocity law in the optically thick part of the atmosphere is not correct.

6. Conclusions

This paper presents the first line blanketed non-LTE model of a Wolf-Rayet star with a hydrodynamically calculated velocity structure for the outer atmosphere. The model solves half of the wind momentum problem of a Wolf-Rayet star by driving its wind in the optically thin part of the atmosphere. The velocity structure in the optically thick part could not be explained. *The calculations presented in this paper reproduce the observed helium lines of HD 50896 in shape and strength.* The following parameters are determined for HD 50896:

$$
\begin{aligned}
L &= 5.5 \cdot 10^5\ \mathrm{L}_\odot \\
M &= 20\ \mathrm{M}_\odot \\
R_{\mathrm{phot}} &= 18\ \mathrm{R}\odot \\
(R_* &= 3.5\ \mathrm{R}_\odot) \\
(T_* &= 84,000\ \mathrm{kK}) \\
\dot{M} &= 3.2 \cdot 10^{-5}\ \mathrm{M}_\odot \mathrm{yr}^{-1} \\
v_\infty &= 2060\ \mathrm{km\,s}^{-1} \\
v_{\mathrm{phot}} &= 1100\ \mathrm{km\,s}^{-1} \\
v_{\mathrm{rad}} &= 100\ \mathrm{km\,s}^{-1} \\
C &\approx 4 \\
f &\approx 1 \cdot 10^{-4},
\end{aligned}
$$

where C is the clumping factor and f the factor that describes the loss of photons from the He II λ303 line. The values given in brackets, T_* and R_*, depend on the adopted velocity law in the optically thick atmosphere and therefore, these values are uncertain. The calculated velocity structure differs considerably from the commonly assumed velocity law with β = 1. A direct consequence of the calculated velocity law is that a higher terminal velocity of the wind is derived than obtained in previous determinations. The newly determined parameters of HD 50896 imply a momentum transfer from the radiation field to the wind of six times the single scattering limit. This is considerable lower than previous estimates of this ratio, which have been in the range from 40 to 100. With this new low ratio, the Wolf-Rayet winds are no longer a class on their own but they form now an extension of the O and Of/WN9 winds, representing the extreme end of the radiation driven winds. Since the WN5 star HD 50896 is among the Wolf-Rayet stars with the strongest observed lines its wind is probably also an extreme example among Wolf-Rayet winds.

The calculations presented here explain only half of the wind acceleration. The creation and the first part of the acceleration has still to be attributed to an unknown mechanism. However, I suspect this is a problem of the present line list, which may still not be sufficiently complete for high ionization stages. Therefore, it is possible that future calculations will be able to explain the whole Wolf-Rayet wind by radiation pressure. If the creation of the Wolf-Rayet wind is also due to radiation pressure then

this would imply that Wolf-Rayet winds also depend on metallicity as predicted for O stars (Kudritzki et al. 1987). Interestingly, such a metallicity dependence is predicted by Vanbeveren (1995) from Wolf-Rayet number statistics.

The key assumption that allowed the calculation of the present model is photon loss from the He II λ303 line. I have proposed (Schmutz 1995) that a Bowen-type fluorescence mechanism removes a small fraction of photons from the radiation field of the He II Lyα resonance line. The spectroscopic analysis presented here empirically determines the photon loss factor to be $f \approx 10^4$. This value is an good agreement with a theoretically calculated factor that is also of the order of $f^* \approx 10^4$ in the critical region where He^{++} recombines. The photon loss is identified to be due to about half a dozen metal transitions.

The photon loss makes He^{2+} recombine closer to the photosphere. This brings an increase in radiation force. A spectroscopic analysis of HD 50896 including photon loss yields a larger luminosity for the Wolf-Rayet star than previous determinations. The increase in luminosity is one contribution to bring the ratio of wind momentum to radiation momentum to more "normal" values. The other contribution comes from the assumption of a clumped wind. A clumped wind allows to explain the observed line strengths with a lower mass loss rate than when using a homogeneous wind. As already pointed out by Hillier (1991b), a clumped wind is required by the observed line profiles, which have less strong electron scattering wings than predicted for homogeneous models.

It has been noted by Howarth & Schmutz (1992) that luminosities of Wolf-Rayet binaries derived with the standard analyses seem to be systematicly too low by a factor of about two when compared with luminosities inferred from their masses using the theoretical mass-luminosity relation. The increase in luminosity of the present model for HD 50896 is a factor of two, roughly, when compared to previous analyses. The bolometric correction for HD 50896 star is now B.C. = -5.0 mag. This value is -0.5 larger than the bolometric correction that was estimated for a WN5 star by Smith et al. (1994) from cluster and association membership and evolutionary models. However, the sample of Smith et al. (1994) includes only one star, HD 4004, that is comparable to HD 50896 and for this star they give only a lower limit. Thus, the luminosity favored here does not disagree with the estimates of Smith et al. (1994) and it is in better agreement with the expectations from stellar evolution models than the old luminosity determinations.

The ultimate diagnostic test, which any proposed model has to pass, is the agreement of the predicted spectrum with the observed spectrum. The line profile fits that have been presented here strongly support the hydrodynamical calculation of the velocity law from the photosphere out to the terminal velocity. This indicates that the evaluation of the radiation force is reasonably good for the ionization stages present in this region. On the other hand, the radiation force in the optically thick atmosphere turns out to be insufficient and therefore, the evaluation of the radiation force at deeper layers, i.e. for high ionization stages, is questionable. Thus, it will be interesting to analyze cooler Wolf-Rayet stars, where the high ionization stages are of less importance. The WNL+abs and Of/WN9 stars, where there is indication that the wind is transparent down to very low velocities, are prime targets for future investigations.

Acknowledgements. I thank Profs. Harry Nussbaumer and Steve Shore for valuable discussions and editorial comments and Dr. Paul Crowther for his improvement of the the ripple correction of my optical observations with the echelle spectrograph CASPEC at ESO. I am most grateful to Dr. Ivan Hubeny. In addition to many important ideas he also provided program codes for the calculation of metal line opacities. I also thank Dr. John Hillier. The first ideas to the kind of work presented here came up in the numerous discussions during our common stay in Boulder.

Appendix A: definition of the photon loss factor

The mean intensity in a spectral line is given by

$$\begin{aligned}\bar{J} &= \int_\nu \phi_\nu \, J_\nu \, d\nu \\ &= \int_\nu \phi_\nu \, \frac{1}{2} \int_\mu \int_\tau S(\nu,\mu,\tau)\, e^{-\tau(\nu,\mu)}\, d\tau \, d\mu \, d\nu \,. \end{aligned} \tag{A1}$$

Without loss of insight we may ignore the influence of the integrals $\int d\mu$ and $\int d\tau$. The transfer and angle integrals average the photon loss factor over a more or less extended region, depending on the optical thickness of the line, and these integrals could be added to the formula given below, if necessary. For an optically very thick resonance line the simplification, $J_\nu = S_\nu$, is certainly nearly exact. Thus, for the He II λ303 line Eq. A1 reduces to

$$\bar{J}^{\rm He} = \int_\nu \frac{\epsilon^{\rm He}\phi_\nu^{\rm He} + \sum_i \epsilon^{{\rm m}_i}\phi_\nu^i + \epsilon^{\rm c}}{\chi^{\rm He}\phi_\nu^{\rm He} + \sum_i \chi^{{\rm m}_i}\phi_\nu^i + \chi^{\rm c}} \, \phi_\nu^{\rm He} \, d\nu \,, \tag{A2}$$

where $\epsilon^{\rm He}$, $\epsilon^{\rm m}$, and $\epsilon^{\rm c}$ are the emissivities in the line center due to the helium transition, of contributing metal transitions m_i, and continuum processes, respectively; the χ's are the corresponding absorption coefficients, and the ϕ's are the line profile functions.

If $\bar{J}^*$ denotes the mean intensity without the influence of metals,

$$\bar{J}^* = \int_\nu \frac{\epsilon^{\rm He}\phi_\nu^{\rm He} + \epsilon^{\rm c}}{\chi^{\rm He}\phi_\nu^{\rm He} + \chi^{\rm c}} \, \phi_\nu^{\rm He} \, d\nu \,, \tag{A3}$$

then Eq. A2 may be written in the form

$$\bar{J}^{\rm He} = (1 - f^*)\, \bar{J}^* \,, \tag{A4}$$

with f^* the loss factor of photons from the radiation field of the helium line. The comparison of Eqs. A2, A3, and A4 yields the definition of the photon loss factor,

$$f^* = 1 - \frac{\bar{J}^{\rm He}}{\bar{J}^*} \,. \tag{A5}$$

Instead of one photon loss factor we may introduce several factors, one factor for the line photons that are absorbed by metal

lines, the capture factor $f^{\rm cap}$, and one for each metal transition, m_i, for their contribution to the mean intensity in the helium line, the contribution factors f^{m_i}. Eq. A2 is then split into two terms,

$$\bar{J}^{\rm He} = \int_\nu \frac{\epsilon^{\rm He}\phi_\nu^{\rm He} + \epsilon^{\rm c}}{\chi^{\rm He}\phi_\nu^{\rm He} + \sum_i \chi^{m_i}\phi_\nu^i + \chi^{\rm c}}\,\phi_\nu^{\rm He}\,d\nu + \int_\nu \frac{\sum_i \epsilon^{m_i}\phi_\nu^i}{\chi^{\rm He}\phi_\nu^{\rm He} + \sum_i \chi^{m_i}\phi_\nu^i + \chi^{\rm c}}\,\phi_\nu^{\rm He}\,d\nu\,. \quad \text{(A6)}$$

Use of the capture factor and contribution factors reduces Eq. A6 to the compact form

$$\bar{J}^{\rm He} = (1 - f^{\rm cap})\,\bar{J}^* + \sum_i f^{m_i}\,\frac{\epsilon^{m_i}}{\chi^{m_i}}\,. \quad \text{(A7)}$$

The capture factor $f^{\rm cap}$ is given by

$$f^{\rm cap} = \frac{1}{\bar{J}^*}\int_\nu \frac{\sum_i \chi^{m_i}\phi_\nu^i}{\chi^{\rm He}\phi_\nu^{\rm He} + \sum_i \chi^{m_i}\phi_\nu^i + \chi^{\rm c}} \times \frac{\epsilon^{\rm He}\phi_\nu^{\rm He} + \epsilon^{\rm c}}{\chi^{\rm He}\phi_\nu^{\rm He} + \chi^{\rm c}}\,\phi_\nu^{\rm He}\,d\nu\,, \quad \text{(A8)}$$

and the contribution factors, f^{m_i}, by

$$f^{m_i} = \int_\nu \frac{\chi^{m_i}\phi_\nu^i}{\chi^{\rm He}\phi_\nu^{\rm He} + \sum_i \chi^{m_i}\phi_\nu^i + \chi^{\rm c}}\,\phi_\nu^{\rm He}\,d\nu\,. \quad \text{(A9)}$$

A comparison of the form of Eq. A7 with Eq. A4 gives the photon loss factor f^* in terms of the capture factor, $f^{\rm cap}$, and contribution factors, f^{m_i}:

$$f^* = f^{\rm cap} - \sum_i f^{m_i}\,\frac{S^{m_i}}{\bar{J}^*}\,. \quad \text{(A10)}$$

Since χ and ϵ are positive numbers the photon loss is always smaller than the capture probability $f^* \le f^{\rm cap}$. It is interesting to note that when the helium line radiation field is close to zero, i.e. when the helium line is a strong absorption line, then most likely, $S^{m_i} > \bar{J}^*$. In this case the contribution of photons from metal transitions can be expected to dominate over the loss of photons, i.e. $f^* < 0$.

If the contribution of the continuum terms are unimportant for the evaluation of the integral in Eq. A8 then the helium line source function can be taken out of the integral and cancels with $\bar{J}^*$. For the optically very thick helium resonance line this is the case and thus, the capture factor, $f^{\rm cap}$, can be approximated by

$$f^{\rm cap} \approx \gamma = \int_\nu \frac{\sum_i \chi^{m_i}\phi_\nu^i}{\chi^{\rm He}\phi_\nu^{\rm He} + \sum_i \chi^{m_i}\phi_\nu^i + \chi^{\rm c}}\,\phi_\nu^{\rm He}\,d\nu\,. \quad \text{(A11)}$$

The approximate capture probability, γ, is identical to the form given by Lucy et al. (1991).

It is worthwhile to note that if the metal line opacities dominate over the helium line opacity at the line centers of the metal lines, then these terms act like delta functions in the integral and Eq. A11 simplifies to

$$f^{\rm cap} \approx \sum_i \phi_\nu^{\rm He}(\nu = \nu_{m_i}^0)\,. \quad \text{(A12)}$$

Thus, in a first approximation, the capture factor depends only on the frequency separation from the helium line center of the strongest metal lines.

If the level populations are in LTE then we find that $f^{\rm cap} = \gamma$ and since $\sum_i f^{m_i} = \gamma$ we find

$$\bar{J}^{\rm He} = (1 - f^{\rm cap})\,\bar{J}^* + f^{\rm cap}\,B_\nu\,. \quad \text{(A13)}$$

In the optically thick case, when $\bar{J}^* \longrightarrow B_\nu$ the capture rate is exactly balanced by contributions from metal line photons, thus $f^* \longrightarrow 0$.

References

Abbott D.C., 1980, ApJ 242 1183
Abbott D.C., Lucy L., 1985, ApJ 288 679
Antokhin I.I., Marchenko S.V., Moffat A.F.J., 1995. In: van der Hucht K.A., Williams P.M. (eds.) Proc. IAU Symp. 163, Wolf-Rayet Stars: Binaries, Colliding Winds, Evolution. Kluver, Dordrecht, p. 520
Bowen I.S., 1935, ApJ 81, 1
Cassinelli J.P., Cohen D.H., MacFarlane J.J., Drew J.E., Lynas-Grey A.E., Hoare M.G., Vallerga J.V., Welsh B.Y., Vedder P.W., Hubeny I., Lanz T., 1996, ApJ 460, 949
Castor J.I., Abbott D.C., Klein R.I., 1975, ApJ 195, 157
Cherepashchuk A.M., Koenigsberger G., Marchenko S.V., Moffat A.E.J., 1995, A&A 293, 142
Crowther P.A., PhD Thesis, University College London, 1993
Dalton M.J., Crowther P.A., Willis A.J., 1995. In: van der Hucht K.A., Williams P.M. (eds.) Proc. IAU Symp. 163, Wolf-Rayet Stars: Binaries, Colliding Winds, Evolution. Kluver, Dordrecht, p. 154
Eaton J., Henry G.W. 1994, IBVS 4061
Ebbets D., 1979, PASP 91, 804
Esteban C., Smith L.J., Vilchez J.M., Clegg R.E.S., 1994, A&A, 272, 299
Feldmeier A., 1995, A&A 299, 523
Friend D.B., Castor J.I., 1983, ApJ 272, 259
Gayley K.G., Owocki S.P., 1995, ApJ, 446, 801
Hamann W.-R., 1987. In: Kalkofen W. (ed.) Numerical Radiative Transfer. Cambridge University Press, Cambridge, p. 35
Hamann W.-R., Schmutz W., 1987, A&A 174, 173
Hamann W.-R., Schmutz W., Wessolowski U., 1988, A&A 194, 190
Hamann W.-R., Koesterke L., Wessolowski U., 1993, A&A 274, 397
Hamann W.-R., Koesterke L., Wessolowski U., 1995, A&A, 299, 151
Hillier D.J., 1987, ApJS 63, 965
Hillier D.J., 1988, ApJ 327, 822
Hillier D.J., 1991a, Theory of Wolf-Rayet Atmospheres. In: van der Hucht K.A., Hidayat B. (eds.) Proc. IAU Symp. 143, Wolf-Rayet Stars and Interrelations with Other Massive Stars in Galaxies. Kluver, Dordrecht, p. 59
Hillier D.J., 1991b, A&A 247, 455
Hogg D.E., 1989, AJ 98, 282
Howarth I.D., Philips A.P., 1986, MNRAS 222, 809
Howarth I.D., Schmutz W., 1992, A&A 261, 503
Howarth I.D., Schmutz W., 1995, A&A 294, 529
Iglesias C.A., Rogers F.G., Wilson B.G., 1992, ApJ 397, 717
Koenigsberger G., Auer L.H., 1985, ApJ 297, 255
Kato M., Hachisu I. 1994, ApJ 437, 802
Kudritzki R.P., Pauldrach A., Puls J., 1987, A&A 173, 293
Langer N., 1989, A&A 220, 135
Leitherer C., Robert C., 1991, ApJ 377, 629
Lucy L., Abbott D.C., 1993, ApJ 405, 738 (LA)

Lucy L., Danziger I.J., Gouiffes C., 1991, A&A 243, 223
Marchenko S.V., Moffat A.F.J., Koenigsberger G., 1994, ApJ 422, 810
Moffat A.F.J., Robert C., 1994, ApJ 421, 310
Mihalas D., 1978 Stellar Atmospheres, (2nd ed.), San Francisco, Freeman
Niedzielski A., 1994, A&A 282, 529
Nugis T., Sapar A., 1985, SvAL, 11, 188
Owocki S.P, 1991. In: U. Heber, C.S. Jeffery (eds.) The atmospheres of early type stars. Springer, Berlin, p. 393
Owocki S.P, Castor J.I., Rybicki G.B., 1988, ApJ 335, 914
Prinja R.K., Barlow M.J., Howarth I.D., 1990, ApJ 361, 607
Puls J., Pauldrach A., 1991. In: Crivillary L., Hubeny I., Hummer D.G. (eds.) NATO ASI Series C 341, Stellar Atmospheres: Beyond Classical Models. Kluver, Dordrecht, p. 175
Robert C., Moffat A.F.J., Drissen L., Lamontagne R., Seggewiss W., Niemela V.S., Cerruti M.A., Barrett P., Bailey J., Garcia J., Topia S., 1992 ApJ 397, 277
Rybicki G.B., Owocki S.P., Castor J.I. 1990, ApJ 349, 274
Schaerer D., Maeder A., 1992, A&A 263, 129
Schaerer D., Schmutz W., 1994, A&A 288, 231
Schaerer D., de Koter A., Schmutz W., 1995. In: S.J. Adelman, W.L. Wiese (eds.) ASP Conf. Series Vol 78, Applications of Powerful New Atomic Databases, p. 467
Schmutz W., 1991, Non-LTE Analysis of Hot Stars Including Line-Blanketing. In: Crivillary L., Hubeny I., Hummer D.G. (eds.) NATO ASI Series C 341, Stellar Atmospheres: Beyond Classical Models. Kluver, Dordrecht, p. 191
Schmutz W., 1994, Space Sci. Rev. 66, 253
Schmutz W., 1995, Observations versus atmospheric models of Wolf-Rayet stars. In: van der Hucht K.A., Williams P.M. (eds.) Proc. IAU Symp. 163, Wolf-Rayet Stars: Binaries, Colliding Winds, Evolution. Kluver, Dordrecht, p. 127
Schmutz W., Hamann W.-R., 1986, A&AL 166, L11
Schmutz W., Hamann W.-R., Wessolowski U., 1989, A&A 210, 236
Schmutz W., Leitherer C., Gruenwald R., 1992, PASP 104, 1164
Schulte-Ladbeck R.E., Mead M.R., Hillier D.J., 1992. In: Drissen L., Leitherer C., Nota A. (eds.) ASPC 22, Nonisotropic and Variable Outflows from Stars, p. 118
Smith L.F., Meynet G., Mermilliod J.-C., 1994, A&A 287, 835
Springmann U., 1994, A&A 289, 505
St.-Louis N., Moffat A.F.J., Drissen L., Bastien P., Robert C., 1988, ApJ 330, 286
Underhill A.B., Grieve G.R., Louth H., 1990, PASP, 102, 749
Vanbeveren D., 1995, A&A 294, 107
Wessolowski U., Schmutz W., Hamann W.-R., 1988, A&A 194, 160
Willis A.J., 1982, MNRAS 198, 897

This article was processed by the author using Springer-Verlag LaTeX A&A style file *L-AA* version 3.